Analysing The Structure And Mechanical Stability Of Amyloid Fibrils Using Atomic Force Microscopy

Biochemistry
MSc by Research 2017/18

Saskia Davis

Supervisor: Dr Wei-Feng Xue

Word count: 14,139

Declaration:

No part of this thesis has been submitted in support of an application for any degree or other qualification of the University of Kent, or any other University or Institution of learning.

ACKNOWLEDGEMENTS

I would like to thank Wei-Feng for this opportunity and all his guidance, Nadia for all her advice and for use of her $A\beta_{42}$ scans, Tracey for her help and support producing and purifying proteins in the lab, Niken, Tansy and Rita for their positive attitudes, Ricardo Marchante for his work on Sup35NM mutants that preceded this project and project students Jade, Katie, Mario and Tam for use of their protein samples. I would also like to thank my friends and family for all their advice and encouragement.

CONTENTS

ABBREVIATIONS

$A\beta_{(42)}$	Amyloid beta (residues 1-42)
AD	Alzheimer's Disease
AFM	Atomic Force Microscopy
APP	Amyloid Precursor Protein
BSE	Bovine Spongiform Encephalopathy
CJD	Creutzfeldt-Jakob Disease
CV	Column Volume
DNA	Deoxyribonucleic Acid
EM	Electron Microscopy
GDP	Gross Domestic Product
His_6-tag	Histidine Tag
HSP104	Heat Shock Protein 104
IPTG	Isopropyl β-D-1-thiogalactopyranoside
NMR	Nuclear Magnetic Resonance
NTFs	Neurofibrillary Tangles
OPR	Oligiopeptide Repeat Region
PD	Parkinson's disease
PDF	Probability Density Function
PFD	Prion Forming Domain
[*PNM*]	[*PSI* No More]
Prion	Proteinaceous infectious particle
QNR	Gln/Asn-rich region in Sup35
ssNMR	solid state Nuclear Magnetic Resonance
Sup35NM	Sup35 (residues 1-253)
ThT	Thioflavin T
TSEs	Transmissible Spongiform Encephalopathies
WT	Wild Type
5FOA	5 Fluoroorotic Acid

ABSTRACT

Prions are proteins that have an ‘infectious’ pathogenic form capable of spreading from cell to cell without involvement of DNA. Prions share a characteristic cross β structure, meaning they belong to a class of protein assemblies called amyloid. Amyloid assemblies are subject of intense research due to their association with neurodegenerative diseases, such as Alzheimer’s and Parkinson’s disease. Mechanical stability is a pertinent factor to consider in the study of prions and prion-like amyloid proteins. The more liable a fibril is to fragmentation, the more readily it can form toxic and/or transmittable particles, which are able to propagate their conformation between cells, consequently enabling the spread of pathology in disease. This project used atomic force microscopy to collect image data of the amyloid fibrils formed from Amyloid-beta peptide and Sup35 protein. First, peptides derived from disease-associated Amyloid-beta fibrils and non-disease-associated Sup35NM were compared to identify what features underpinned the disparity in transmissibility and disease-association between the two types of amyloid. Secondly, the presence and position of a His-tag was confirmed not to have a significant effect on suprastructure or stability of Sup35NM particles. Finally, three mutants of Sup35NM with a single amino acid substitution in a region crucial for prion propagation were investigated to find the extent to which structure affected infective transmissibility. The structural changes that occurred in fibrils under mechanical stress were elucidated and thus their mechanical stability. Exploring the structure and the mechanisms responsible for amyloid disease pathology and prion spread is of vital importance, as it has clinical relevance in the pursuit of effective therapies for debilitating conditions, such as Alzheimer’s and Parkinson’s disease.

1. INTRODUCTION

1.1 Prions and Prion-Like Proteins

1.1.1 The Protein-Only Hypothesis

It was first theorised that certain proteins could replicate in the absence of nucleic acid as a genetic blueprint in 1982 (Prusiner, 1982; Diaz-Espinoza and Soto, 2010; Zabel and Reid, 2015). Stanley Prusiner named this class of remarkable proteins 'prions' for proteinaceous infectious particles (Prusiner, 1982; Hauw, Haik and Brandel, 2015; Das and Zou, 2016). The 'protein-only hypothesis' postulates that prions have the ability to self-propagate, replicating their form by recruiting and converting a previously physiological protein with a native conformation to a misfolded disease-associated isoform and consequently initiating aggregation (Soto and Castilla, 2004; Ma and Wang, 2014).

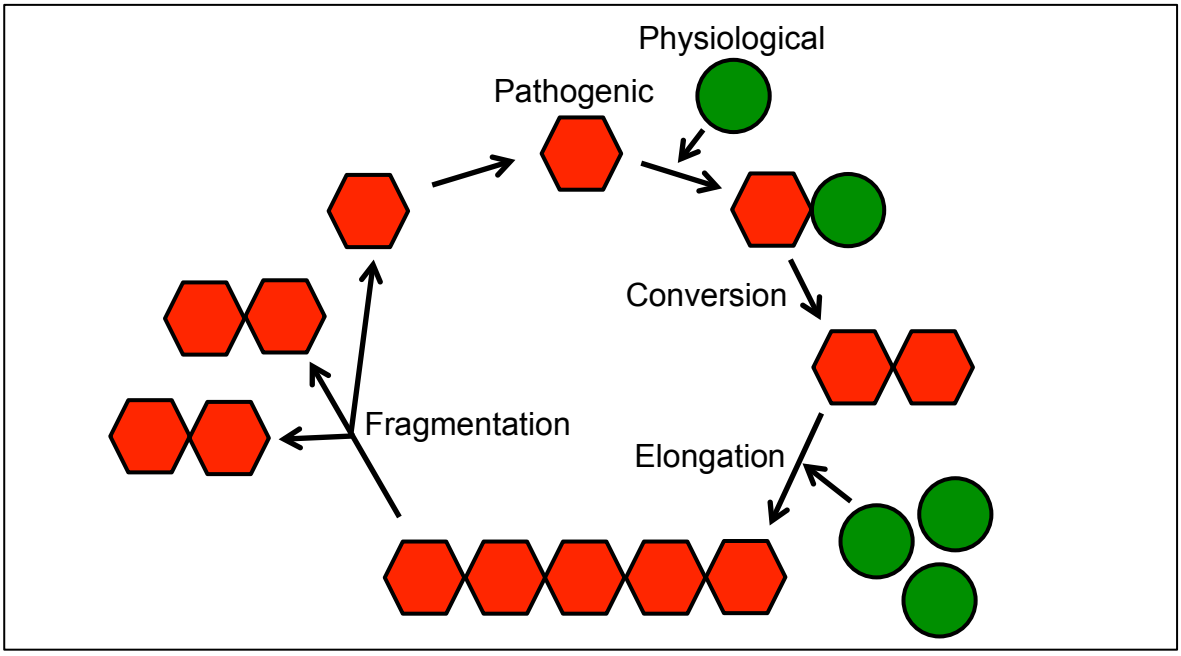

Figure 1 - Simplified schematic of prion propagation and seeding in the protein-only hypothesis. A pathogenic protein recruits its physiological counterpart and converts it to its pathological form. This initiates elongation, which is later followed by fragmentation and consequently the production of more seeds. This rapid amplification results in aggregation and propagation of the amyloid.

All prions aggregate to form fibrils with a characteristic cross β structure, meaning they belong to a class of proteins called amyloid. It is important to note that while all prions are amyloid, not all amyloid are prions or even pathogenic (Rambaran and Serpell, 2008). In this project, the underlying cause of this variation in the pathogenic potential of amyloid was investigated.

Unsurprisingly, the protein-only hypothesis was met with fierce criticism following years of the protein vs. nucleic acid debate, which was seemingly resolved with the Watson-Crick discovery of the genetic code in 1953 (Zabel and Reid, 2015). The prion hypothesis contradicted everything the scientific community had come to accept. Fortunately, abundant and compelling evidence now exists in support of prions and their existence is widely recognised, but a debate on the exact definition, scope, and mechanism of a 'prion' continues to this day (Colby and Prusiner, 2011).

1.1.2 Prion vs. Prion-Like

Initially, the term prion was used to describe the protein responsible for the transmissible spongiform encephalopathies (TSEs), a group of fatal neurodegenerative diseases that spread between sheep as Scrapie, to cows as Bovine Spongiform Encephalopathy (BSE), and to humans as Creutzfeldt-Jakob disease (CJD) (Cutlip *et al.*, 1994; Mathiason, 2017). TSEs are infectious in the traditional sense that they can spread between individuals and even species. It has since been demonstrated that disease-associated mammalian amyloid aggregates formed by Amyloid beta (Aβ), Tau, α-synuclein, TAR DNA-binding protein 43, and huntingtin, also possess the self propagating properties of a prion and can 'infect' neighbouring cells *within* the same individual, but not spread *between* individuals (except in rare cases such as blood transfusions and

administration of contaminated human growth hormone) (MacKenzie *et al.*, 2002; McCutcheon *et al.*, 2011; Andréoletti *et al.*, 2012; Appleby *et al.*, 2013; Zhang, Nie and Chen, 2018). Debate continues as to whether intercellular 'infection' can or should be considered 'infectious' giving rise to terms such as 'prion-like' and prionoid, in an attempt to acknowledge that some amyloid exhibit infectious qualities (Liberski, 2012; Moore, Faris and Priola, 2015; Abbott, 2016; Annus, Csáti and Vécsei, 2016).

1.1.3 Broader Implications

Regrettably, there is currently no cure for CJD, but it is not considered an imminent threat as it is extremely rare; less than 10 cases have been recorded in the last 6 years worldwide (Diack *et al.*, 2014; Ironside, Ritchie and Head, 2017; Seed *et al.*, 2018). Despite this, amyloid and specifically prions continue to be the subject of intense research; this is due to their connection with neurodegenerative diseases such as Alzheimer's disease (AD) and Parkinson's disease (PD) (Diack *et al.*, 2014; Fraser, 2014; Hauw, Haik and Brandel, 2015; Abbott, 2016; Ironside, Ritchie and Head, 2017; Seed *et al.*, 2018).

The basis for this variation in the infectious potential between different amyloid is still unknown; in this study the suprastructure (which includes fibril height, length and overall appearance) and mechanical stability was investigated as a possible source of the inconsistency in transmission potential between prion Sup35 and disease-associated prion-like mammalian protein $A\beta_{42}$, which is implicated in AD.

1.2 Alzheimer's Disease

1.2.1 Physical And Molecular Manifestations

AD is a progressive neurodegenerative disease characterised most notably by insidious cognitive decline and behavioural symptoms such as dementia, hallucinations, delusions, aggression and depression (Shanthi, Krishnan and Rani, 2015; Dubois *et al.*, 2016; Serafini *et al.*, 2016). On a cellular level, a significant amount of neuronal loss can be found in several regions of the brain, accompanied by extracellular aggregates of Aβ called neuritic plaques and hyper-phosphorylated Tau protein aggregates called neurofibrillary tangles (NTFs) (Brion, 1998; Blennow, de Leon and Zetterberg, 2006). It is understood that neuropathological changes (such as Aβ plaques and NFTs) occur long before symptomatic cognitive impairment and dementia are detected (Shanthi, Krishnan and Rani, 2015). These observations lead to the amyloid cascade hypothesis, which suggests that aggregation of Aβ is the initiating factor that later triggers cell abnormities such as inflammation and oxidative stress that culminates in dysfunction, degeneration and ultimately the death of neuronal cells (Verdile *et al.*, 2004).

1.2.2 Socio-Economic Implications

Primarily a disease of the elderly, AD affects 5% of those over 65, and up to 33% in those over 85. It was estimated in 2010 that 36 million people were living with AD and this figure is predicted to rise to 66 million by 2030, and to 81 million by 2040, following an anticipated increase in life expectancy by virtue of advancements in medicine and living conditions. Deaths from stroke and heart diseases are decreasing, whereas deaths attributed to AD are rising. The cost of dementia, of which AD is a primary cause, is estimated to be in excess of $600 billion per year, which is equivalent to more than 1% of gross domestic product

(GDP), and can be expected to double by 2040 (Blennow, de Leon and Zetterberg, 2006; Pouryamout *et al.*, 2012; McCarthy, 2013; Sibener *et al.*, 2014; Marešová *et al.*, 2015; Marešová, Klímová and Kuča, 2015; Alzheimer's Association, 2016). This data highlights the substantial financial and emotional burden caused by AD, and the escalating demand for a cure.

1.2.3 Search For A Cure

There is no therapy available today that can prevent or halt the disease process in AD. Current therapies are limited to temporarily mitigating the cognitive and behavioural symptoms of AD; acetylcholinesterase inhibitors for example work by increasing the amount of available neurotransmitter acetylcholine (Voisin and Vellas, 2009; Bond *et al.*, 2012). Many avenues such as rodent and zebrafish animal models have been extensively explored in a fruitless attempt to elucidate the mechanistic underpinnings of AD (Lieschke and Currie, 2007). Antibodies, once seen as the most promising prospect have also thus far been unrewarding. Active anti-Aβ immunotherapies were shown to clear brain Aβ deposits but have been discontinued as it caused meningoencephalitis in 6% of AD patients treated (Panza *et al.*, 2014).

It is conceivable that the lack of effective treatment for AD over 100 years after its discovery is due to the lack of focus on amyloid structure and how the mutual structure of amyloid fibrils enables prion/prion-like propagation and spread, the mechanisms of which have yet to be elucidated in detail (Verdile *et al.*, 2004; Mangialasche *et al.*, 2010; Kumar, Singh and Ekavali, 2015). In this study, the correlation of structure and mechanical stability of $A\beta_{42}$ and Sup35NM variants with infective potential was considered.

1.3 Amyloid Fibril Structure

1.3.1 Amyloid Fibrils

Amyloid fibrils are widespread in nature and extremely diverse in function, from cell protection and structure, to protein control and storage, all undeniably important biological roles (Pham, Kwan and Sunde, 2014). Many soluble proteins can aggregate to form insoluble amyloid fibrils, which all share a cross β structure and common properties, despite being formed from different precursor proteins that don't share sequence homology or related native structure (Serpell, Sunde and Blake, 1997; Nelson *et al.*, 2005; Nelson and Eisenberg, 2006b). The structure, function, and interaction of amyloid fibrils are of significance as Aβ and Tau, associated with AD, aggregate to form amyloid fibrils (Tycko, 2006; Sawaya *et al.*, 2007). Light microscope studies first identified amyloid fibrils using Congo red dye (see Figure 2c below) over 150 years ago (Sipe and Cohen, 2000; Frid, Anisimov and Popovic, 2007). The structure of amyloid fibrils has since been determined in atomic resolution.

1.3.2 Biophysical Methods And Structure

The structure of amyloid fibrils has been studied using, to name a few, electron microscopy (EM), X-ray fibre diffraction and crystallography, solid-state NMR (ssNMR), and atomic force microscopy (AFM) (Jahn *et al.*, 2010; Stroud *et al.*, 2012). By definition, amyloid fibrils are layers of cross β sheets stacked perpendicular to the axis of the fibril. Each layer is associated with its neighbouring layers by side chains protruding from each sheet, these form complementary steric zippers, and are further supported by hydrogen bonding (Nelson *et al.*, 2005; Nelson and Eisenberg, 2006a; Sawaya *et al.*, 2007; Biancalana, Makabe and Koide, 2010).

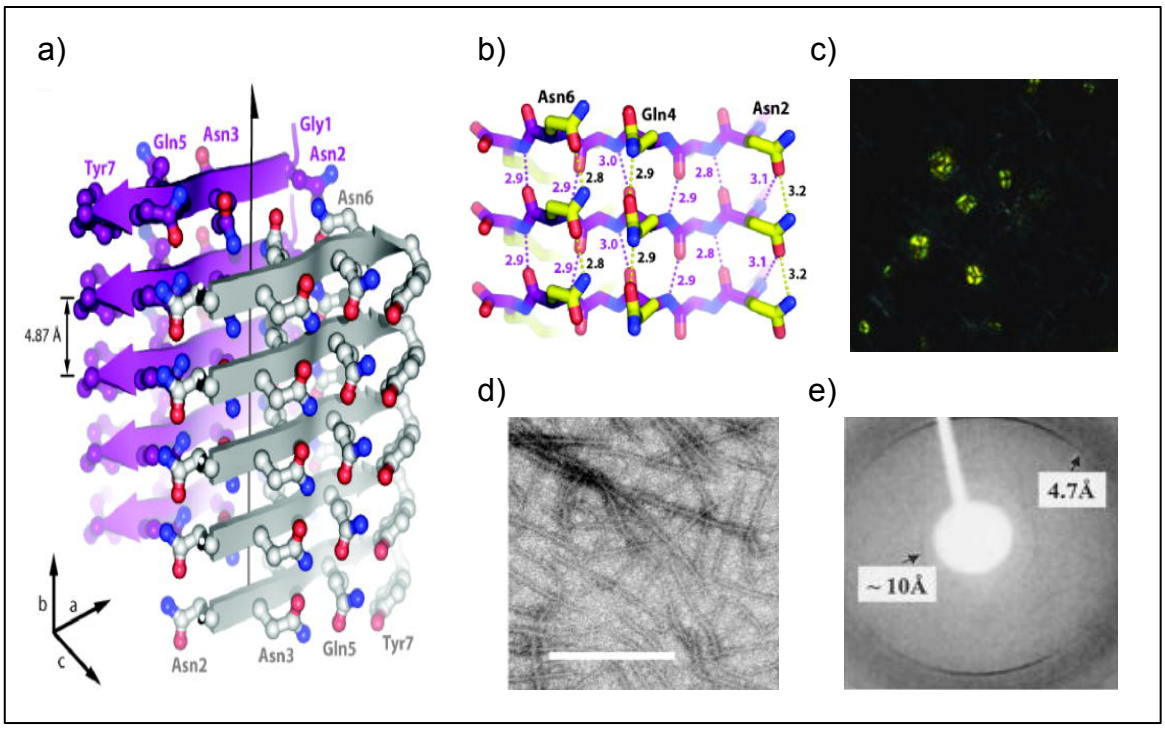

Figure 2 - Biophysical investigations of amyloid structure. a) Amyloid fibril schematic based on ssNMR and X-ray crystal analysis. The backbone of each β strand is shown as a thick arrow, perpendicular to the direction of the fibril. Protruding balls and sticks depict sidechains. Inter-strand separation is 4.87 Å, adapted from: (Nelson et al., 2005). b) Detailed amyloid fibril schematic based on ssNMR and x-ray crystal analysis. Schematic highlights the placement of inter-strand hydrogen bonds (yellow dots), the *length of each hydrogen bond is given in Å units, adapted from: (Nelson et al., 2005). c) Congo red positive Aβ plaques from coronal brain sections of a 12-month-old 5XFAD mouse (400X magnification) adapted from: (Rajamohamedsait and Sigurdsson, 2012). d) Negatively stained transmission EM image of Sup35NM fibrils, scale bar 200 nm, adapted from: (Tycko and Wickner, 2013). e) X-ray diffraction pattern of a Sup35NM fragment. The meridional reflections at 4.7 Å and equatorial reflections at ~ 10 Å are characteristic of the amyloid cross β structure, adapted from: (Balbirnie, Grothe and Eisenberg, 2001).*

These biophysical investigations have all contributed detail to our understanding of amyloid, and therefore prion structure. Specifically, X-ray diffraction patterns have revealed that fibrils form highly ordered, closely packed, dehydrated, parallel stranded beta sheets held by a steric zipper (Sunde *et al.*, 1997; Balbirnie, Grothe and Eisenberg, 2001; Diaz-Avalos *et al.*, 2003; Morris and Serpell, 2012). Studies utilising ssNMR have helped map the amyloid fibrils architecture, such as the torsional angles and interatomic distances between amino acids residues (Tycko, 2000, 2006; Madine *et al.*, 2008; Tycko and Wickner, 2013). Molecular and atomic detail can be supported and given context by investigation of morphology using EM and AFM, which reveal fibrils are ~ 6-10 nm wide, straight and unbranching (Antzutkin *et al.*, 2002; Stromer and Serpell, 2005; Xu, 2009; Tycko and Wickner, 2013). Investigation of suprastructure on a mesoscopic level (using AFM and EM) fuels our understanding of the seeding and elongation mechanisms that enable prion and prion-like propagation.

1.3.3 Fibril assembly

It is widely accepted that amyloid fibrils form by a nucleation-dependent polymerisation mechanism, composed of nucleation followed by elongation (Serpell, 2000). Analogous to classical nucleation theory, it is thought that the smallest species that can grow into a fibril, the nucleus, is thermodynamically unstable (Kashchiev, 2015; Chatani and Yamamoto, 2018). Secondary processes: fragmentation and secondary nucleation (which occur on preformed fibrils, after the initial formation of amyloid fibrils by primary nucleation), are of particular significance in disease-associated amyloid fibrils they yield oligomers, which are thought to be one of the cytotoxic species of amyloid (Cremades *et al.*, 2012; Cohen *et al.*, 2013; Xue, 2015). A relationship between reduced fibril length caused by fibril fragmentation and enhanced cytotoxic potential has been

established in β2m fibrils (Xue, Homans and Radford, 2008, 2009; Xue *et al.*, 2010; Marshall *et al.*, 2014). The relationship between fibril dimensions and ability to propagate was explored in this thesis by analysing and comparing the structure and mechanical stability of $A\beta_{42}$, Sup35NM and variants of Sup35NM.

1.3.4 Mechanical stress

All amyloid fibrils have the same core structure, despite different precursor proteins; the question remains why amyloid assemblies range from cytotoxic to benign and vary in transmissibility. It follows that the less mechanically stable a fibril is along the length of its axis, the more liable it is to fragmentation, and thus the greater the potential for seeding and cell to cell transmission (Wogulis *et al.*, 2005; Xue, Homans and Radford, 2008; Xue *et al.*, 2010; Kayed and Lasagna-Reeves, 2012; Kraus, Groveman and Caughey, 2013; Marshall *et al.*, 2014). The aim of this thesis was to establish a link between changes in structure and impact on transmissibility using new data that recorded the effect of mutations and perturbation by controlled sonication on both the structure and mechanical stability of fibrils and data previously collected on prion transfection efficiency *in vivo* (Xue and Radford, 2013; Marshall *et al.*, 2014; Marchante *et al.*, 2017).

1.4 Proteins

1.4.1 Amyloid beta

Proteolytic cleavage of amyloid precursor protein (APP) by γ-secretase produces Aβ peptides. The resulting Aβ peptides are 39-42 amino acids in length, prone to aggregation, and a fundamental constituent of pathogenic plaques (Bolduc *et al.*, 2016). The imprecise cleavage of APP by γ-secretase results in two main proteolytic products: $A\beta_{40}$, which is 40 residues long, and $A\beta_{42}$, which is 42 residues long. The concentration of $A\beta_{40}$ is several times more than the concentration of $A\beta_{42}$ in the cerebral spinal fluid, and yet $A\beta_{42}$ is the main component of amyloid plaques in AD. In fact, $A\beta_{40}$ is only detected in a small percentage of plaques, suggesting the initial plaque formation does not involve $A\beta_{40}$ (Gu and Guo, 2013). As such $A\beta_{42}$ was selected to focus on during these investigations.

The amyloid cascade hypothesis states that plaques consisting of insoluble aggregates of Aβ are responsible for AD; this was the leading theory for decades. Despite this, there is an inexplicable lack of correlation between the local concentration of plaques and extent of neuronal death. Evidence now suggests small soluble Aβ oligomers, rather than plaques, may be responsible for the cytotoxic effect seen in AD. Oligomers can be seen as intermediates between monomers and highly ordered fibrillar structures, they are found in rapid equilibrium *in vivo* (Ono, Condron and Teplow, 2009). Aβ oligomers exist over a wide molecular weight, ranging from below 10 kDa to above 100 kDa. Even oligomers with similar atomic weights vary in morphology; this has been demonstrated in studies that reveal structure-specific antibodies do not universally bind oligomers (Sakono and Zako, 2010).

It is now believed that, rather than being the source of cytotoxicity, the infamous plaques found in AD may essentially act as a reservoir of oligomers, the true cytotoxic species. This hypothesis is supported by evidence that there is a strong positive correlation between local oligomer concentration and extent of synaptic damage and loss. Many studies now highlight soluble oligomers as the causative agents of AD, nevertheless it remains unclear what particular characteristics of oligomers, their structure, mechanical stability and mechanisms make them so transmissible and cytotoxic (Sakono and Zako, 2010).

1.4.2 Tau

Physiologically, Tau is a microtubule-associated protein that helps maintain the neuronal network in the brain (Kumar *et al.*, 2015). Abnormal phosphorylation of Tau affects its normal function and has an impact on neuron viability (Lee and Leugers, 2012). It has been found that Aβ oligomers trigger hyper-phosphorylation of Tau, which in turn leads to the formation of toxic neurofibrillary tangles (NFTs) implicated in AD (Kumar *et al.*, 2015). This connection reinforced the importance of investigating $A\beta_{42}$.

1.4.3 Sup35NM And Mutant Variants

The yeast prion Sup35 is used as a model to study structure and function of disease-associated mammalian prion-like proteins as it shares a structure and a similar mechanism of propagation, but is tolerated by yeast cells, so investigation can occur without cell death. The reported impact of Sup35 varies from neutral to the cell, to beneficial (Wickner *et al.*, 2015). As such, Sup35 was used as a comparison for disease-associated $A\beta_{42}$ to see if the disparity in transmissibility and toxicity between the two amyloid proteins had a structural basis.

Following this, the impact of a single amino acid substitution in three Sup35NM mutants was investigated. The mutations (G58X) were located in a region that was highlighted as crucial for prion propagation. The sequence of a Sup35 protein can be divided into three main sections: The C-terminal, which is critical for the translation termination function of the prion, a middle region, which is highly charged and imperative to the stability of the prion, and the prion-forming domain (PFD) at the N-terminal.

The Sup35NM (N terminal) domain used in these investigations is necessary and sufficient for seeding, propagation and generations of prion strains, which exhibit different characteristics. The Sup35NM PFD, which is similar in sequence to mammalian prion protein, contains an oligiopeptide repeat region (OPR), where the single amino acid substitutions were located. Specifically, the OPR is thought to contribute to propagation by promoting fragmentation (Tuite, 2000; Parham, Resende and Tuite, 2001; Marchante *et al.*, 2013a; Bondarev *et al.*, 2014).

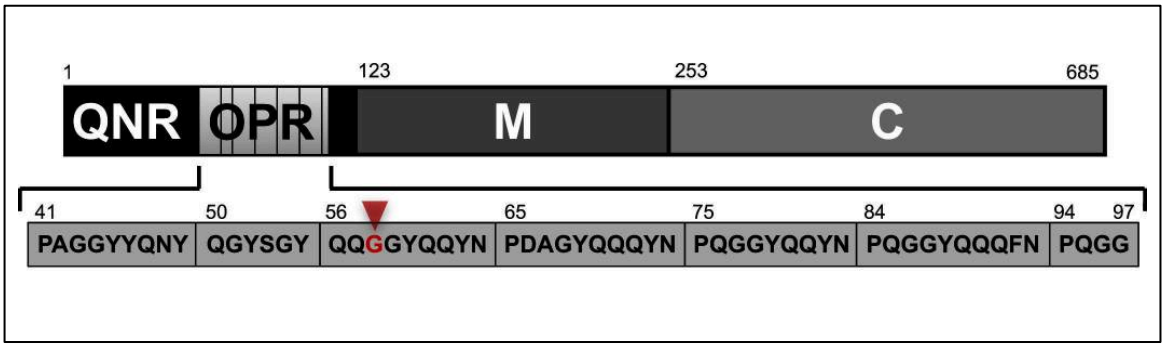

Figure 3 – Schematic of the Sup35 protein and placement of mutation. Sup35NM consists of (residues 1–253), including PFD (residues 1-97), which consists of the QNR (a Gln/Asn-rich region) and the OPR. The mutations are located in the OPR (indicated by the red arrow). The highly charged middle region 'M' is vital for the mitotic stability of the prion. Adapted from: (Marchante et al., 2013b).

1.5 AFM

Atomic force microscopy (AFM) is a powerful nano-scale analysis tool. It exploits the interaction between atoms of the sample and the scanning probe. The probe oscillates over the surface of the sample and feeds back data to map a three-dimensional topographic, this information is not attainable by any other biophysical tool. AFM has the capability to produce high-resolution images, comparable to EM, but with the advantage of only requiring ambient conditions, ideal for observing biological structures (Ushiki, 2001; Allison *et al.*, 2010; Vahabi, Nazemi Salman and Javanmard, 2013; de Pablo and Carrión-Vázquez, 2014).

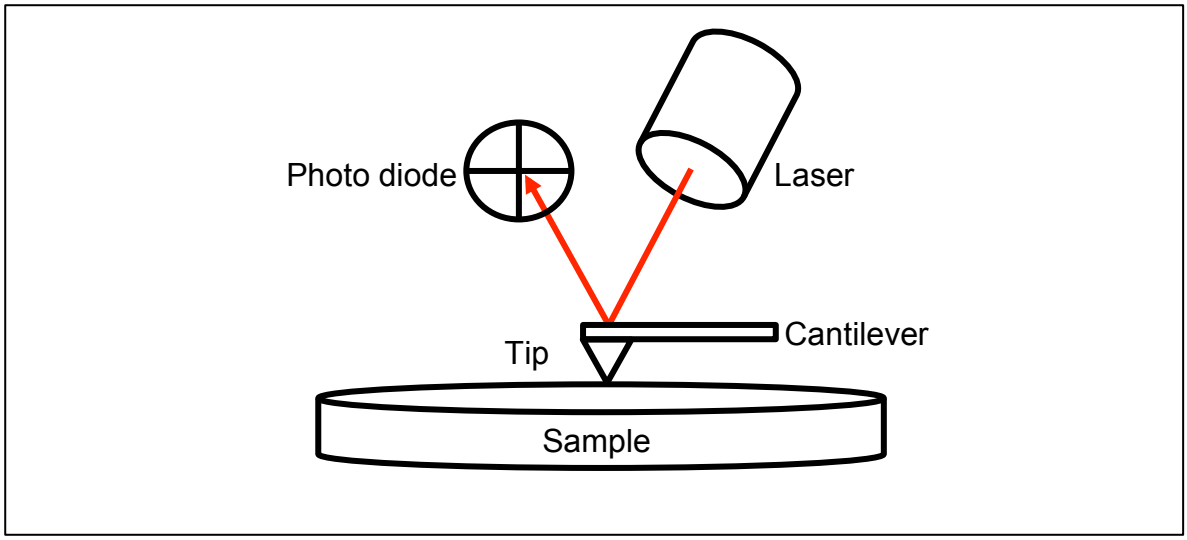

Figure 4 - Simplified AFM schematic. Basic components of AFM shown: a laser beam deflects off the back of the cantilever and attached tip, the laser deflections are measured by a photo-sensitive photodiode detector and fed back to a data processor (not shown here).

The silicone nitride probe tip scans the sample in the x y plane, recording the height of the sample (z). Small repulsive forces between atoms in the probe tip and atoms on the surface of the sample cause deflections that are detected and measured by laser tracking. A position sensitive photodiode measures deflections

on an atomic level to give the height of the sample. The position of the probe is adjusted based on feedback from the height of the sample (Jensen, 2013; Morkvėnaitė-Vilkončienė, Ramanavičienė and Ramanavičius, 2013).

This highly sensitive equipment was used to monitor the height, length and suprastructure (overall appearance on mesoscopic level) of fibrils. This data was then used to to compare disease-associated and non-disease-associated fibrils to determine the extent to which structure and mechanical stability had an impact on transmissibility and cytotoxicity.

1.6 Aims

The aim of this project was to analyse and compare the structure and mechanical stability of amyloid fibrils using atomic force microscopy (AFM). First $A\beta_{42}$ and Sup35NM were compared to see if there was any disparity between their suprastructure and mechanical stability that would explain how, despite both being amyloid assemblies, the two proteins possessed different levels of transmissibility and cytotoxicity.

Additionally, the rarely considered effect of protein purification tags was investigated. The structure and mechanically stability of C-terminal His-tag and N-terminal His-tag fibrils were compared to ensure that the addition of 6 residues to either terminus had no effect, as has been discovered for some proteins.

Sup35NM mutants with a single amino acid substitution in the OPR, known to be crucial for prion propagation were then considered. Fibril height and length data following perturbation by controlled sonication was used to make an assessment of mechanical stability, and this was combined with pre-existing data on the seeding potential of the mutants *in vivo,* to come to a conclusion on the extent of the effect of structure and mechanical stability on prion propagation.

This thesis investigated the theory that long sonication periods result in a reduction in fibril length, but maintenance of fibril height and thus enable transmissibility and cytotoxicity (Wogulis *et al.*, 2005; Xue, Homans and Radford, 2008; Marshall and Serpell, 2009; Xue *et al.*, 2009, 2010; Marshall *et al.*, 2014). Theoretically, prions must have low mechanic strength along the length of the fibril to fragment, but high mechanical strength perpendicular to the axis of the fibril to maintain height. The height of the particle must be conserved to allow

the particle to act as a seed, physical nucleus and template for elongation in the course of prion/prion-like propagation.

The current lack of effective treatments for debilitating neurodegenerative conditions such as AD warrants a reconsideration of, and focus on, the structure of prions and prion-like proteins and specifically what aspects of their structure facilitate propagation.

2. METHOD & MATERIALS

2.1 Materials

All chemicals used are of the highest grade commercially available.

The region of the Sup35 gene encoding the NM region of the yeast Sup35 protein (residues 1–253) was amplified from plasmid pUKC1620 by PCR and cloned into pET15b as a BamHINdeI fragment. This generated an N-terminal His6-tag fusion protein.

Site-directed mutagenesis of plasmid p6442 (CUP1, SUP35NM-GFP) was performed with the QuikChange to produce Sup35NM G58A G58K G58V mutants. See (Marchante *et al.*, 2013b) for further detail on the Sup35NM G58A G58K G58V mutants.

Amyloid Beta Peptide (residues 1-42) was purchased in 5 mg batches from Bachem (Germany). Monomers were prepared and purified (using gel filtration) as described previously (Hellstrand *et al.*, 2010). Fibril formation, sonication as described below for Sup35NM.

2.2 Sup35NM Protein Expression And Purification

BL21 DE3 was grown overnight in 50 ml LB, supplemented with 0.1 mg/ml ampicillin, and then transferred to 1 L cultures of the same medium. On reaching an OD680 of ~0.5, expression was induced with 1 mM IPTG for 4 hours. Cells were harvested at 6000 rpm and the cell pellets washed in buffer A1 (20 mM Tris-HCl pH 8.0, 1 M NaCl, 20 mM Imidazole). Cells were pelleted and kept at 80℃ for later use. For the affinity purification process, buffer A2 (20 mM Tris-HCl pH 8.0, 1 M NaCl, 20 mM Imidazole, 6 M GdnHCl) was added to the frozen cell

pellets at a 5:1 (v/v) ratio, followed by sonication at an amplitude of 22 microns until the cell pellet was completely disrupted. This solution was then subject to centrifugation at 13000 rpm for 30 minutes, and the resulting supernatant collected. 1 ml of Chelating Sepharose Fast Flow (GE Healthcare) was added to a small plastic column and prepared for affinity purification by sequential washing with one column volume (CV) of water, 0.2 M $NiCl_2$, buffer A1 and buffer A2. The equilibrated resin was then resuspended in buffer A2 and added to the previously collected supernatant. This mixture was then incubated for 1 hour at room temperature with agitation to improve protein binding to the affinity resin. Centrifugation at 5000 rpm was subsequently used to collect the resin, which was then washed in 5 ml buffer A2 and resuspended in buffer A2 and transferred back to the column. After one wash with 1 CV buffer A2, elution was achieved by addition of 4 ml buffer A3 (20 mM Tris-HCl pH 8.0, 1 M NaCl, 0.5 M Imidazole, 6 M GdnHCl). The resulting elute was immediately used in size-exclusion purification, which was run using a HiLoad 16/600 Superdex 200 pg (GE Healthcare) column in an AKTA Prime Plus chromatography system (GE Healthcare). The elute was injected into the size-exclusion column previously equilibrated with 1 CV water followed by 1 CV buffer S1 (20 mM Tris-HCl pH 8.0, 0.5 M NaCl) and 1 CV buffer S2 (20 mM Tris-HCl pH 8.0, 0.5 M NaCl, 6 M GdnHCl). The relevant Sup35NM protein fractions were collected according to the A280 displayed throughout the run, diluted in buffer S2 and used in fibril-forming reactions.

2.3 Sup35NM Fibril Formation

2.5 ml of 20 mM purified Sup35NM were buffer exchanged into Fibril Forming Buffer (20 mM Na_2PO_4 pH 7.4, 50 mM NaCl) using a PD-10 column (GE Healthcare) as per manufacturer's instructions. Protein concentration was

measured using A280 and then adjusted to 10 mM using Fibril Forming Buffer. Protein was aliquoted into Protein LoBind tubes (Eppendorf) and polymerized at 30℃ for at least 48 hours. For monitoring polymerisation, 100 µl samples of protein were aliquoted into black puregrade 96-well plates (Starlab) and Thioflavin T was added to a final concentration of 10 mM. The plate was sealed with Starseal Advanced Polyolefin Film (Starlab) and kinetics were monitored in a FLUOstar OMEGA plate reader (BMG Labtech) at 30℃.

2.4 Controlled Sonication

Fibril fragmentation was achieved by sonication over different periods (indicated in the corresponding figure legend) using a probe sonicator (Qsonica Q125) at 20% amplitude in consecutive 5 s on/off cycles. Eppendorf tube containing 80 µl of protein sample kept in an ice-water bath throughout. A dilution factor of 1:10 before pipetting onto mica employed throughout to minimise the removed volume from the original sample.

2.5 Atomic Force Microscopy

Fibril samples (20 µl) were deposited on mica. After incubation at room temperature, Sup35 samples were washed with 1 ml of 0.2 mm syringe filtered mQH20 and dried under a gentle stream of nitrogen, then left again to incubate overnight before scanning.

Samples were imaged using a Bruker Multimode AFM with a Nanoscope V controller and a ScanAsyst probe with a silicone nitride tip (tip height 2.5–8 mm, tip radius 2 nm, spring constant 0.4 N/m and resonant frequency 70 kHz).

2.6 Image Processing

Images captured at a size and pixels indicated in the figure legend, typically 10 µm x 10 µm and 1024 x 1024 pixels. Images processed using the Nanoscope analysis software (version 1.5, Bruker). Image baseline flattened using baseline correction to remove tilt and bow. Individual particle height analysis completed using the sectioning tool within Nanoscope analysis. Data saved as processed image files and analysed using in-house automated fibril-tracing scripts written in Matlab.

2.7 Data Processing

All images imported and analysed using an in-house fibril-tracing script named Trace_y (version 1.0 July 2014) written in Matlab (version R2017a) (Uversky and Lyubchenko, 2013).

2.7.1 Noise Exclusion

Command line below used to open fibril-tracing software.

```
>> Trace_y
```

Image cropped to the desired size using crop function, file saved as “img” to use in next step. “img” file opened in workspace within Matlab.

Command line below used to produce 3 images, displaying the data selected and the data excluded as noise.

```
>> x = 1:img.pixelPerLineImg;
>> y = 1:img.nLinesImg;
>> z = img.z;
>> [fitSegments, zresidual, zmodel] = TracePolContour(x, y, z, 2, 2);
>> surface([z zmodel zresidual], 'LineStyle', 'none'); colorbar;
```

Suggested variables shown underlined. Variables first tested using a smaller cropped image. The functions of the 2 underlined variables are apparent width and height cut off respectively. Correct variables produce an image consisting of three panels: overall image being analysed, the data to be traced, and data excluded as noise.

2.7.2 Tracing

Following commands used to produce an image of traced fibrils (mapped from start to finish with a line ending in 'x'):

```
>> [particles, f] = LinkSegments(fitSegments, 2, 2, 16, 20, x, y, z);
```

The variables are width, height cut off, normalisation and cut off respectively. Variables changed (suggested variables shown underlined) until all fibrils are traced. Importantly, this command created variable 'particles' in the workspace. This is the number of traced fibrils, their heights and lengths. This data was used to produce histograms.

2.7.3 Distribution Of Height Histogram

Following commands entered to produce a histogram displaying the distribution of the height (found in column 4 of 'particles'):

```
height=(cellfun(@(m) mean(m(:, 4)), particles));
goodIndexes = (height) >= 1.5;
mean(height(goodIndexes))
std(height(goodIndexes))
skewness(height(goodIndexes))
histogram(height(goodIndexes),0:0.5:15, 'Normalization','pdf');
```

Heights below 1.5 nm were excluded as noise using the 'goodIndexes' command line. Steps and upper limit varied, (suggested here 0:0.5:15) depending on expected average and maximum fibril height, an optimised selection produced

a histogram that encompassed the average height and maximum height. Axes were labelled and the scale of the y axis edited to best display data bars (0.4 used throughout). Scale of axes kept constant between figures for ease of comparison.

2.7.4 Distribution Of Length Histogram

Following commands entered to produce a histogram displaying the distribution of the length (found in the last cell of column 6 of 'particles'):

```
lc = cellfun(@(c) c(end,6),particles);
lcum = (lc*9.7656);
goodIndexes = (lcum) >= 9.7656;
mean(lcum(goodIndexes))
std(lcum(goodIndexes))
skewness(lcum(goodIndexes))
histogram(lcum(goodIndexes), 0:25:1000, 'Normalization','pdf');
```

Lengths were originally recorded in **pixels**, not nm, as height was. As such, the length 'lc' was multiplied by resolution to covert length to nm. Resolution was found in the 'img' variable in the matlab workspace, or calculated by original image size (nm)/ 1024 pixels, for example 10,000/1024 = 9.7656. Lengths below 1 pixel or 9.7656 nm were excluded as noise using the 'goodIndexes' command line.

Steps and upper limit were varied (suggested here 0:25:1000) depending on expected average and maximum fibril length; an optimised selection produced a histogram that encompassed the average length and maximum length. Axes were labelled and the scale of the y axis edited to best display data bars (0.04 used throughout). Scale of axes kept constant between figures for ease of comparison.

3. RESULTS

The results of these investigations have been divided into 4 subsections; the first subsection describes the process of optimisation of fibril tracing analysis. The second section details an investigation into the suprastructure and mechanical stability of $A\beta_{42}$ and Sup35NM fibrils. It was found that the two proteins had similar mechanical stability following sonication but appeared slightly different under native conditions. In the third subsection, it was confirmed that the presence and placement of a His-tag had no negative effect on the structure or stability of Sup35NM fibrils. Finally, prion Sup35NM wildtype (WT) fibrils and 3 mutant variants were compared and unexpectedly uncover that G58V was the most similar in appearance and dimensions to the WT, not G58A as expected.

3.1 Fibril Tracing

3.1.1 Optimisation of fibril tracing analysis

In-house fibril tracing software called Trace_y was used to remove noise from each scan, map or 'trace' individual particles and subsequently record their height and lengths for analysis. In order to accurately remove noise and record the dimensions of particles, a set of parameters had to be optimised first. Following a long period of trial and error over a range of possible parameters, optimised parameters (suggested in the methods and materials section) were established using the approach described below. The importance of correct parameters was paramount, as incorrect tracing could have resulted in incorrect height and length data and consequently incorrect conclusions.

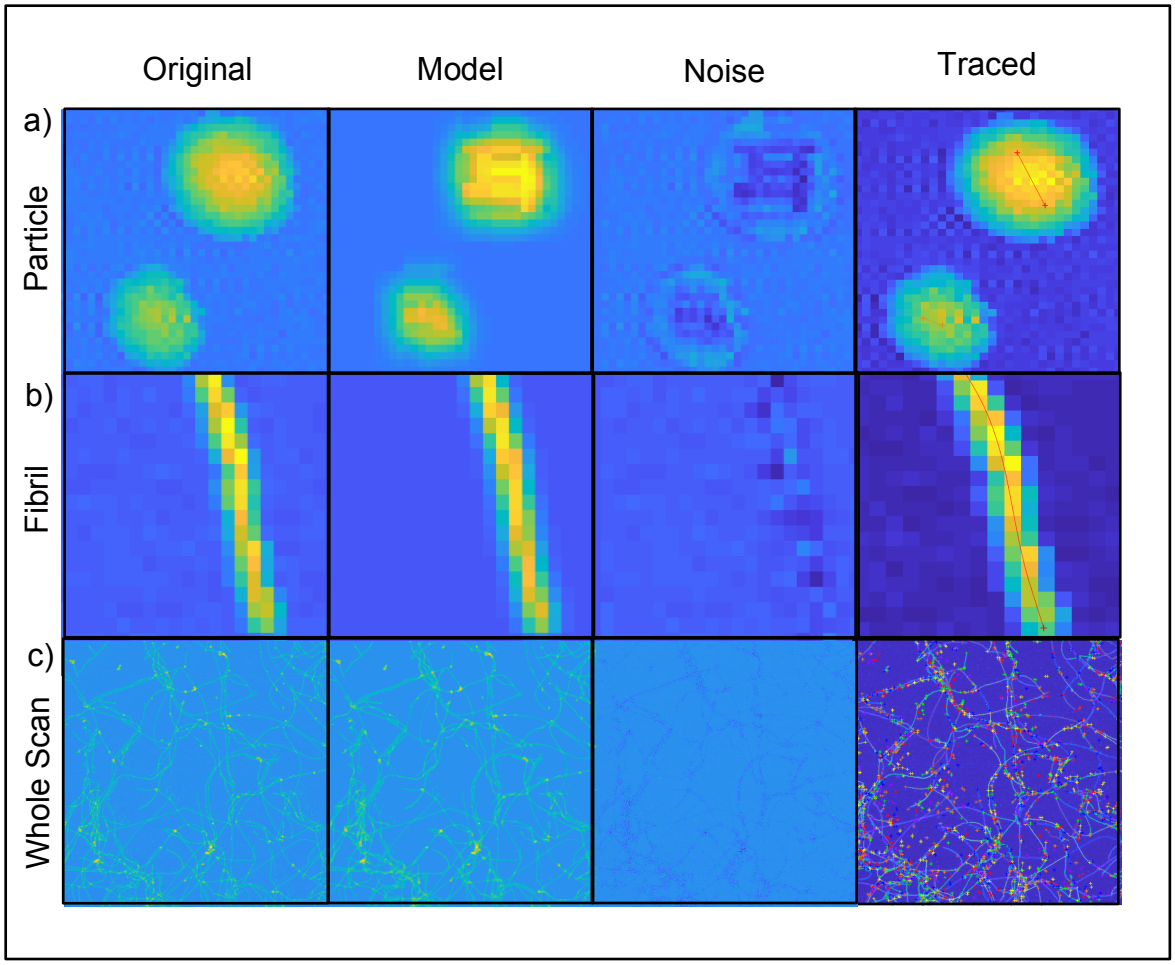

Figure 5 – The first column depicts the original image to be analysed. The second column depicts the desired data that has been selected and the third column depicts the data that has been excluded as noise. The fourth column depicts the particles that have been traced, highlighted by coloured lines. In the examples above all the particles have been traced, indicating the selected parameters have been successful. Once successful parameters have been established on a single particle and single fibril scale, shown in row a) and row b) respectively, the parameters were applied to the whole scan as exemplified in row c) in the figure above. Extensive trial and error, exemplified in appendix 2, led to the suggested parameters listed in the methods and materials section.

3.1.2 Incorrect Parameters

In order for the fibril tracing software to record accurate data, all fibrils and particles had to be identified and traced at this stage. Common issues encountered included a height exclusion parameter that was set too high, which disregarded fibrils as noise, a height exclusion parameter that was set too low, which resulted in background being ‘counted’ as fibrils, and incorrect parameters which resulted in two particles being counted as one, or a traced ‘bend’ in a straight fibril, both of which produced an inaccurate recorded length.

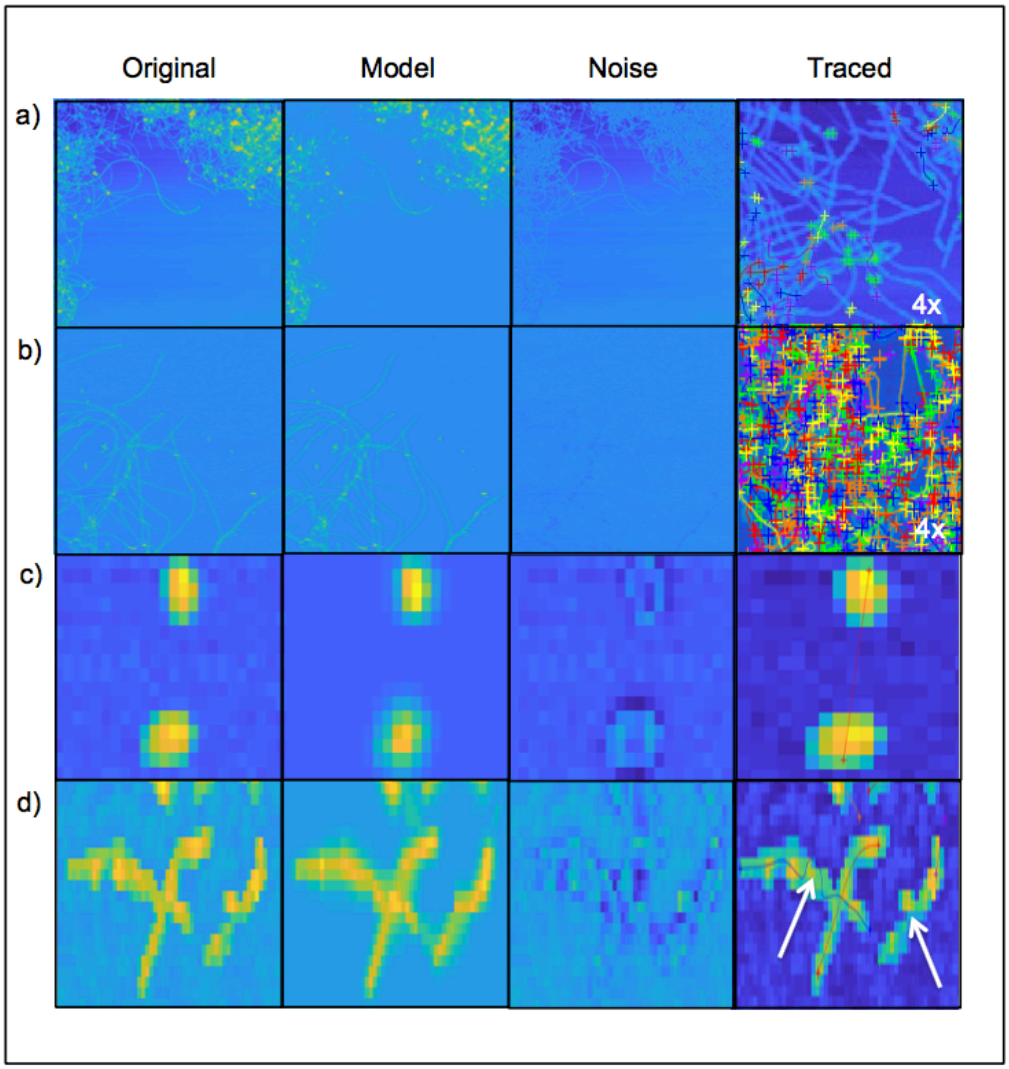

Figure 6 – Examples of issues encountered when optimising parameters for fibril tracing in software Trace_y. Row a) height exclusion parameter set too high, resulted in fibrils being excluded as background noise (third column) and thus fibrils not being traced (fourth column). Magnification x4 used to highlight untraced fibrils. Row b) height exclusion parameter set is too low, resulted in background noise (third column) being 'mistaken' for particles and traced (fourth column). Magnification x4 used to highlight excessive tracing. Row c) incorrect parameters have been used; this resulted in two separate particles being 'counted' as one long fibril. Row d) incorrect parameters have been used. This resulted in a straight fibril being traced with a 'bend' that would result in a longer recorded length than is accurate. White arrows in the fourth column indicate incorrectly traced 'bends' in straight fibrils.

Caveats

Throughout the remaining results section, the datasets (i.e. height and length graphs and averages) are representative of the fibrils in one scan of one sample of each protein, due to the wide scope of fibrils analysed and the time taken to prepare, scan and analyse each sample. Preparing samples and gathering data in triplicate or more would have been ideal given more time; nonetheless, the data presented follows the pattern expected based on currently unpublished data collected by N.Koloteva-Levine, as well as similar fibril dimentions to those found by other biophysical methods explored in Figure 2.

Prior to sonication, fibrils span the entire scan area and extend beyond the reach of the scan area. Due to this, the mean lengths are not accurate prior to sonication for any scan. However, the value can be useful for comparative purposes, for example in Figure 7, $A\beta_{42}$ (Figure 7a) visually has a greater proportion of short fragments than Sup35NM (Figure 7b), and this resulted in a reduced mean length. Where appropriate, mean lengths are written with the notation (>> X nm) (or circled in graphs) to acknowledge that the value is a significant underestimation.

3.2 Comparison of suprastructure and mechanical stability of Sup35NM and $A\beta_{42}$ amyloid fibrils

Utilising these new optimised parameters $A\beta_{42}$, implicated in Alzheimer's disease (AD), and Sup35NM, a yeast prion protein used as a model to investigate the behaviour and structure of amyloid were compared. Images were collected and height and length data of unsonicated $A\beta_{42}$ and Sup35NM fibrils were recorded by AFM to assess if they bore a close resemblance on a mesoscopic level, and progressed to see if they reacted in the same manner under mechanical stress, in the form of controlled sonication. Specifically, high mechanical stability perpendicular to the axis of the fibril and low mechanical stability parallel to the axis of the fibril was expected. This would be characterised by consistency in fibril height across all sonication time points as the fibril fragmented and fibril length decreased.

3.2.1 $A\beta_{42}$ appeared slightly more fragmented than Sup35NM fibrils prior to sonication.

The most striking difference between the suprastructure of $A\beta_{42}$ (Figure 7a) and Sup35NM fibrils (Figure 7b) was that the $A\beta_{42}$ fibrils appeared slightly fragmented even before sonication; in comparison, the Sup35NM fibrils were long, consistent in width, with no apparent fragmentation. Before considering the height and width data recorded by AFM, it was possible to speculate that Sup35NM fibrils were structurally more stable than disease-associated $A\beta_{42}$ fibrils.

Further height and length analysis supported the preliminary assumptions gathered from the images. The mean height for the unsonicated Sup35NM fibrils was 7.0 nm and the mean length was 215.2 nm. Compared to the unsonicated $A\beta_{42}$ fibrils, which had a mean height of 6.3 nm and a mean length of 146.3 nm. The histograms were consistent with the overall appearance of the fibrils as the $A\beta_{42}$ fibrils were much more heterogeneous than the Sup35NM fibrils, reflected in the wide array of heights recorded (Figure 7c).

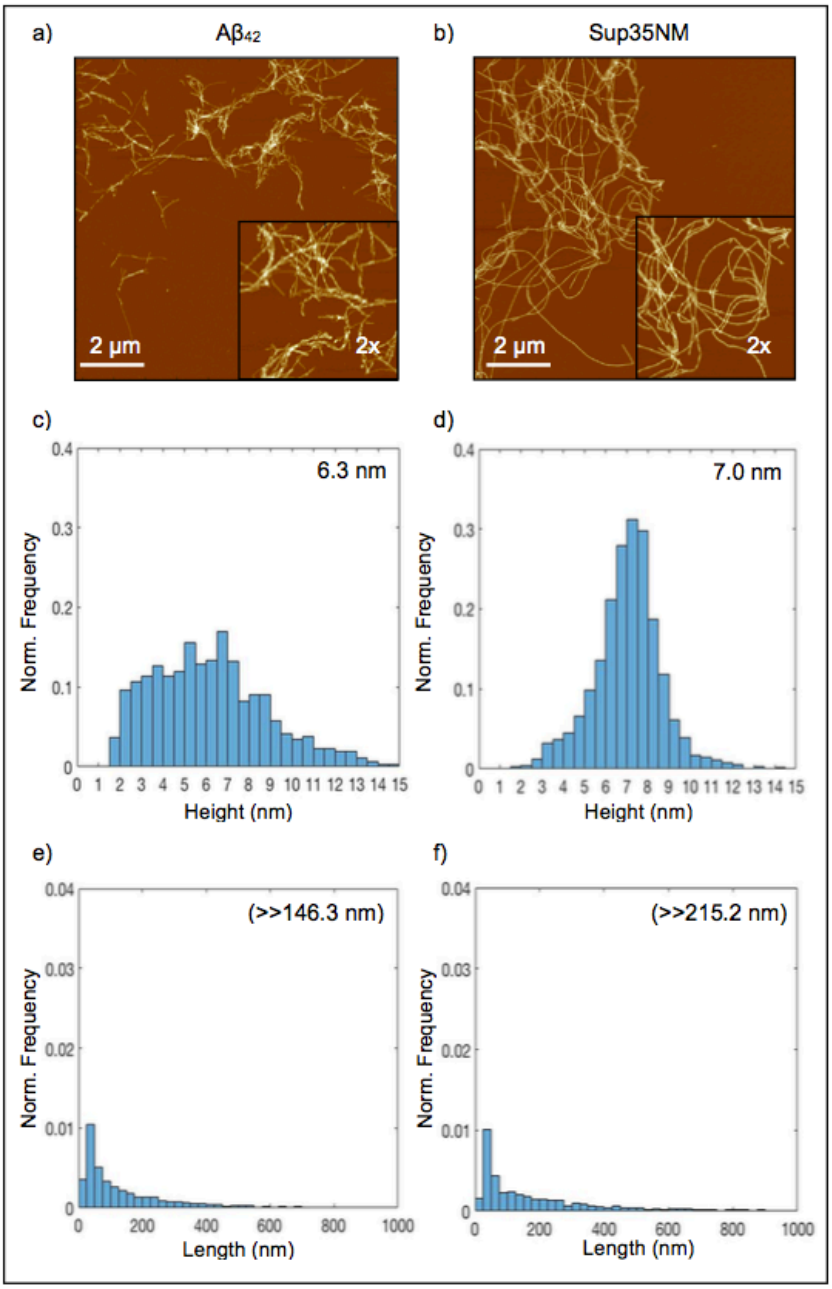

Figure 7 – a) AFM image of Aβ$_{42}$ fibrils (2 μM) on mica. b) AFM image of Sup35NM fibrils (2 μM) on mica. Scan size 10x10 μm 1024 x 1024 pixels, and scale bar represents 2 μm for both images. Images collected by N.Koloteva-Levine. Normalised particle height (nm) distribution of c) Aβ$_{42}$ fibrils d) Sup35NM fibrils. Normalised particle length (nm) distribution of e) Aβ$_{42}$ fibrils f) Sup35NM fibrils. Mean value displayed in the top right. Notation (>> X nm) used to signify fibrils extend outside the scanned area, and thus the value is an underestimation.

3.2.2 $A\beta_{42}$ fibrils appeared more fragmented than Sup35NM fibrils following mild sonication.

Following 5 seconds sonication the $A\beta_{42}$ and Sup35NM particles (Figures 8a and 8b) appeared somewhat alike, both consisted of mostly short but whole fragments. However, the Sup35NM particles were more diverse than the $A\beta_{42}$ particles, containing some longer species, as highlighted in the 2x magnification view. The height and length data recorded from the scans supported these observations, the mean heights for $A\beta_{42}$ and Sup35NM fibrils were 5.5 nm and 5.4 nm respectively, and the mean lengths recorded for $A\beta_{42}$ and Sup35NM fibrils were 131.5 nm and 152.7 nm respectively.

As predicted at the start of this series of experiments, the fibrils fragmented length-wise, but did not “break down” as height remained consistent. These results were an early indication of a connection between the mechanical stability of a fibril and the pathogenic potential of a fibril; specifically that the prion-like mechanism of spread of a fibril such as $A\beta_{42}$ required low mechanical stability in order for the fibrils to form seeds that then acted as a templates and nuclei for the growth of new fibrils.

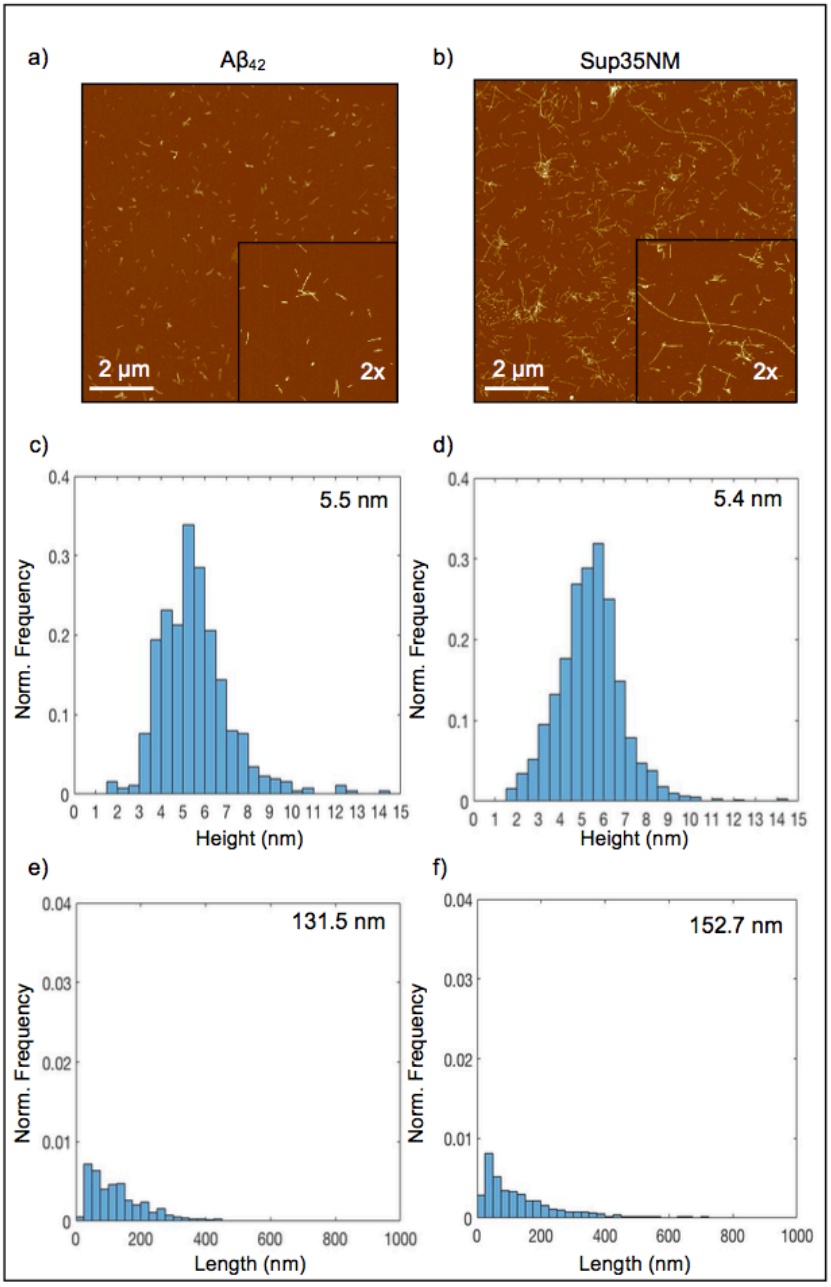

Figure 8 - a) AFM image of Aβ$_{42}$ particles (0.2 μM) following 5 seconds sonication on mica. b) AFM image of Sup35NM particles (0.2 μM) following 5 seconds sonication on mica. Scan size 10x10 μm 1024 x 1024 pixels, and scale bar represents 2 μm for both images. Images collected by N.Koloteva-Levine. Normalised particle height (nm) distribution of c) Aβ$_{42}$ particles d) Sup35NM particles. Normalised particle length (nm) distribution of e) Aβ$_{42}$ particles f) Sup35NM particles. Mean value displayed in the top right.

3.2.3 $A\beta_{42}$ and Sup35NM fibrils both maintained height following extreme sonication.

Again, the average height remained similar between the two samples (Figure 9) and indeed, irrespective of increasing sonication time. A mean height of 5.7 nm was recorded for $A\beta_{42}$ particles and 5.3 nm for Sup35NM particles. As anticipated, the mean lengths of both fibrils were drastically reduced following 300 seconds sonication to 38.5 nm for $A\beta_{42}$ and 42.7 nm for Sup35NM. Although visibly both samples (Figures 9a and 9b) appeared to consist of mainly small and round 'dot-like' particles Sup35NM had a slightly more heterogeneous assortment of particles ranging from 'dots' to slightly longer species highlighted in the 2x magnification view. The heterogeneity in Sup35NM particle length was reflected in the histograms as a greater deviation (Figure 9f), despite the similarities in mean length between the particles.

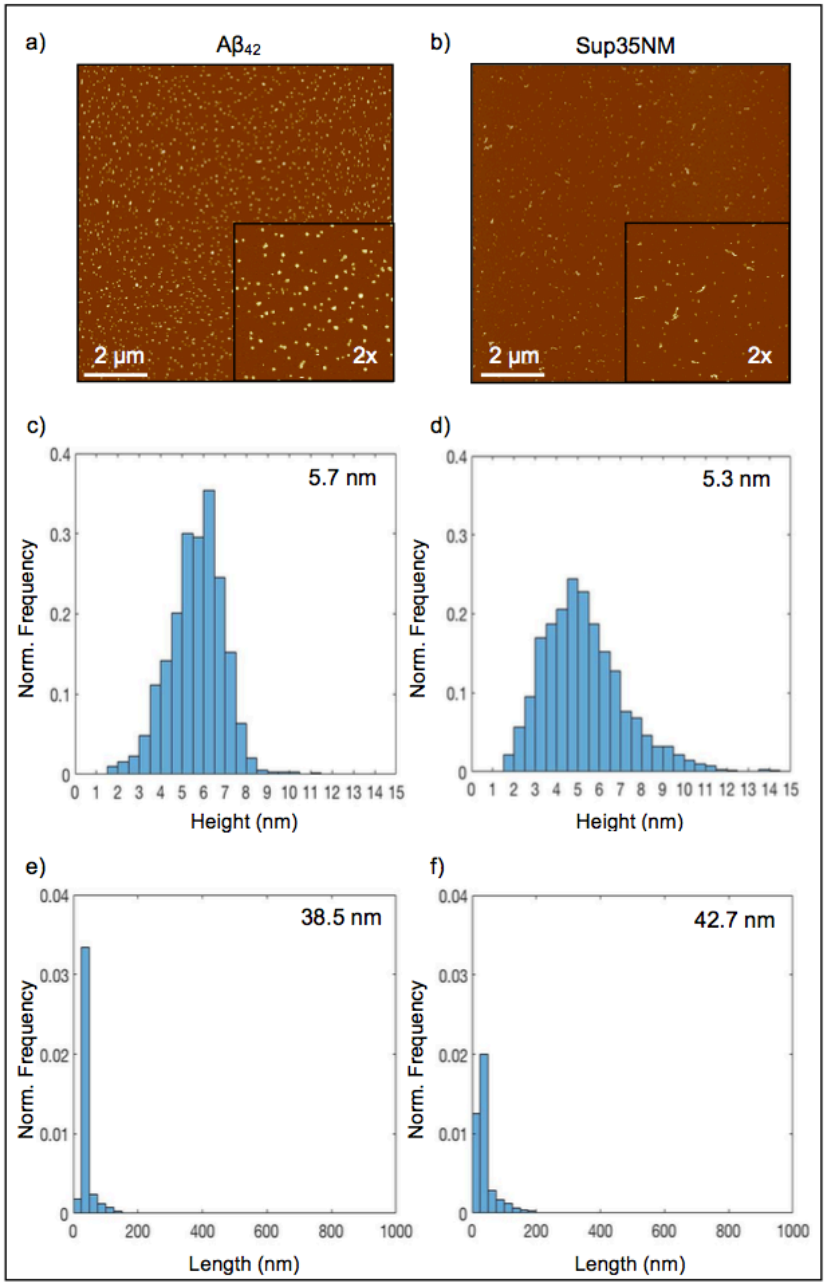

Figure 9 - a) AFM image of Aβ$_{42}$ particles (0.2 µM) following 300 seconds sonication on mica. b) AFM image of Sup35NM particles (0.2 µM) following 300 seconds sonication on mica. Scan size 10x10 µm 1024 x 1024 pixels, and scale bar represents 2 µm for both images. Images collected by N.Koloteva-Levine. Normalised particle height (nm) distribution of c) Aβ$_{42}$ particles d) Sup35NM particles. Normalised particle length (nm) distribution of e) Aβ$_{42}$ particles f) Sup35NM particles. Mean value displayed in the top right.

3.2.4 Comparison of $A\beta_{42}$ and Sup35NM fibril height and length following sonication.

Both visually on a mesoscopic level and with regards to mechanical stability following AFM height and length data analysis, the amyloid fibrils behaved remarkably similar following sonication. As predicated, the heights of the fibrils (Figure 10a) were maintained while lengths decreased (Figure 10b) with each increase in sonication period. The persistence of the height of the amyloid fibrils under such mechanical force was a demonstration of the high mechanical stability perpendicular to the axis of the fibril and indicated the importance of the height to the prion/prion-like mechanism of propagation.

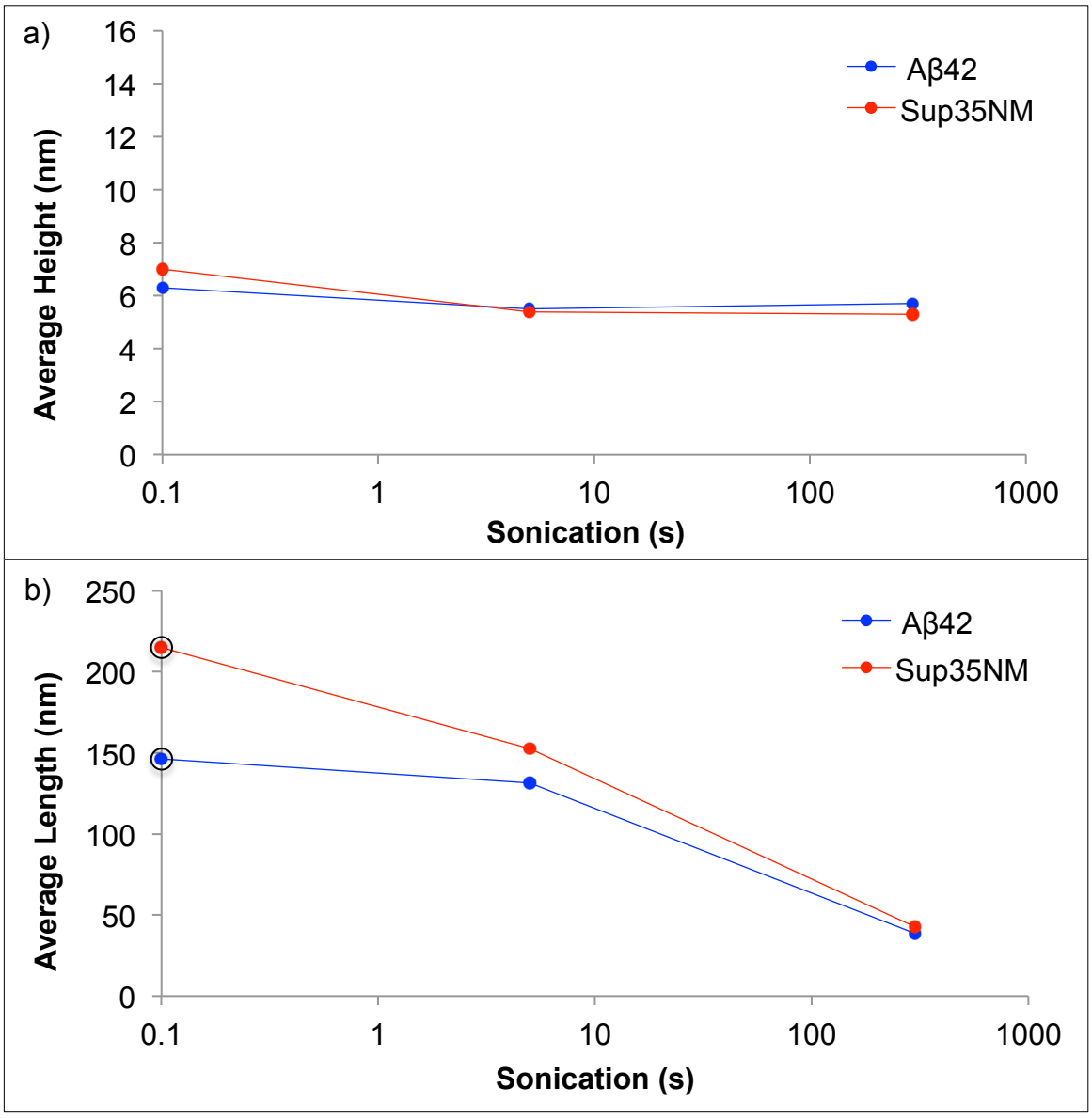

Figure 10 a) Consistent average height (nm) and b) decreasing average length (nm) of Sup35NM and $A\beta_{42}$ particles following 0, 5 and 300 seconds sonication, Sonication time shown on a logarithmic scale for both. Values circled to signify fibrils extend outside the scanned area, and thus the value is an underestimation.

Sonication (s)	Protein	Average Height (nm)	Average Length (nm)
0	$A\beta_{42}$	6.3	(>>146.3)
	Sup35NM	7.0	(>>215.2)
5	$A\beta_{42}$	5.5	131.5
	Sup35NM	5.4	152.7
300	$A\beta_{42}$	5.7	38.5
	Sup35NM	5.3	42.7

Table 1 - Comparison of $A\beta_{42}$ and Sup35NM particles height and length (nm) following 0, 5 and 300 seconds sonication. Notation (>> X) used to signify fibrils extend outside the scanned area, and thus the value is an underestimation.

3.3 The Impact Of A His-tag

The Sup35NM fibrils investigated so far have had an N-terminal His-tag, for purification purposes, but it was yet to be determined if this had an effect on fibril structure and behaviour. As such, Sup35NM WT conventionally used in prion research (which has an N-terminal His-tag) and Sup35NM with a C-terminal His-tag were scanned to assess if there were any inconsistencies on a morphological scale, and then both samples were subjected to a range of sonication periods to see if they behaved the same under mechanical stress. Any major differences, visual or in mechanical stability could have indicated the potential of a His-tag to change the behaviour of the protein, rendering any data previously collected unreliable.

3.3.1 Sup35NM C-terminal His-tag fibrils initially appeared homologous to Sup35NM N-terminal His-tag fibrils.

The unsonicated Sup35NM C-terminal His-tag fibrils (Figure 11a) were near indistinguishable from the Sup35NM N-terminal His-tag fibrils conventionally used, it had long, straight, overlapping but distinct fibrils. The Sup35NM N-terminal His-tag fibrils had a slightly larger diameter with a mean of 7.0 nm, compared to the Sup35NM C-terminal His-tag fibril mean of 6.4 nm, both values fell within the expected range determined by other biophysical methods such as EM and X-ray crystallography explored in Figure 2. Sup35NM N-terminal His-tag fibrils had a mean length of 215.2 nm and Sup35NM C-terminal His-tag fibrils had a mean of 158.1 nm, but as explained previously, average lengths recorded before sonication are not strictly accurate.

After 5 seconds sonication the scanned image and recorded height and length data were atypical. The images collected of Sup35NM C-terminal His-tag fibrils displayed some short distinct fibrils as expected but also a considerable population of amorphous aggregation as highlighted by the 2x magnification view (Figure 11b). The wide diversity of heights and lengths recorded were represented in the irregular histograms (Figures 11d and 11f). The height distribution had a much greater deviation than typically seen. A mean height of 10.5 nm was recorded; unquestionably a consequence of the clumping seen, as exceedingly overlapping fibrils gave a misleadingly large height value. Remarkably, Sup35NM C-terminal His-tag fibrils had a mean length of 158.5 nm, which seamlessly fit the trend and was very similar to its less clumped counterpart. This suggested that the fibrils did indeed sonicate and fragment to form distinct fibrils as anticipated, but perhaps the sample was not plated fast enough and the fibrils irreversibly associated prior to pipetting.

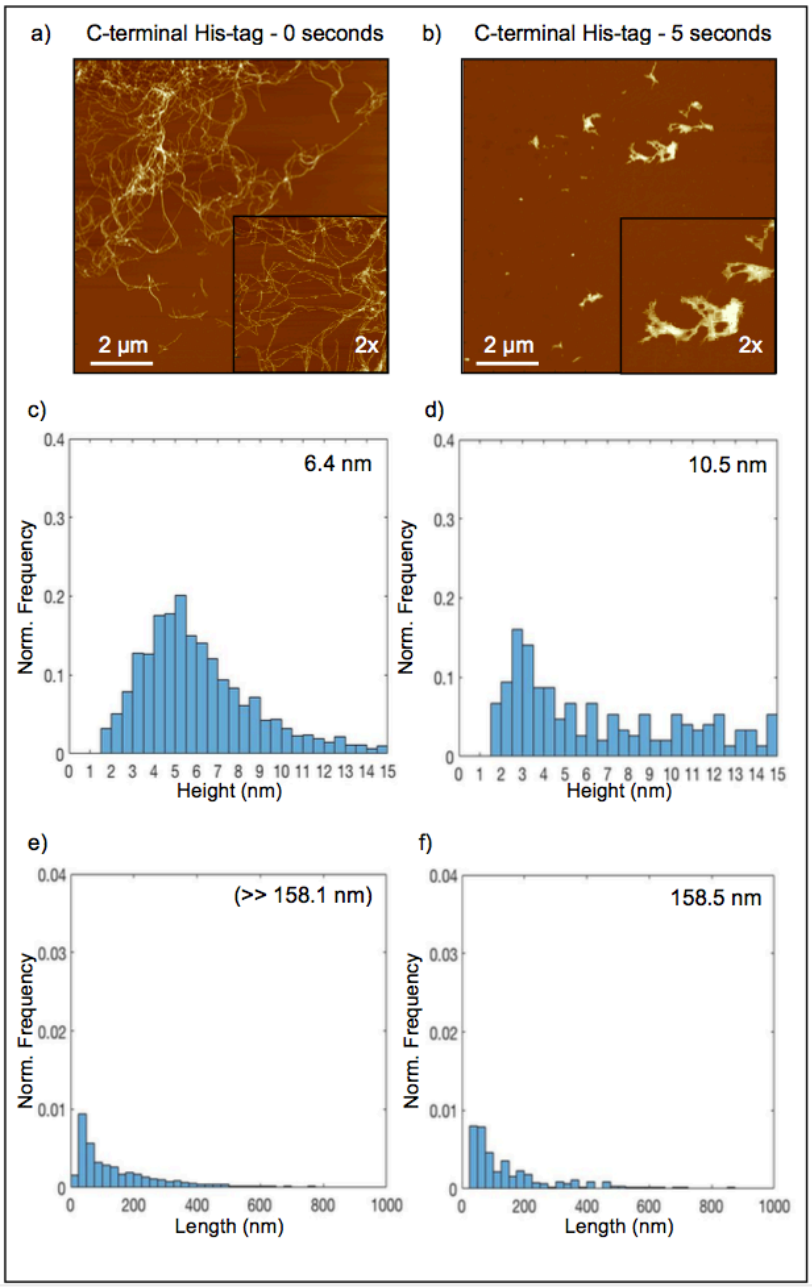

Figure 11 - AFM image of Sup35NM C-terminal His-tag fibrils following a) 0 seconds b) 5 seconds sonication (2 µM and 0.2 µM respectively) on mica. Scan size 10x10 µm 1024 x 1024 pixels, and scale bar represents 2 µm for both images. Images collected by N.Koloteva-Levine. Normalised particle height (nm) distribution of Sup35NM C-terminal His-tag fibrils following c) 0 seconds d) 5 seconds sonication. Normalised particle length (nm) distribution of Sup35NM C-terminal His-tag fibrils following e) 0 seconds f) 5 seconds sonication. Mean value displayed in the top right. Notation (>> X nm) used to signify fibrils extend outside the scanned area, and thus the value is an underestimation.

3.3.2 Individual analysis of C-terminal His-tag particles revealed heights that followed the pattern expected.

Discrete particles outside the main body of clumping had heights between 5 and 6 nm, confirming the theory that the average height measurement recorded by AFM was a result of clumping, as oppose to actual particle height. These results suggested height was not affected by sonication.

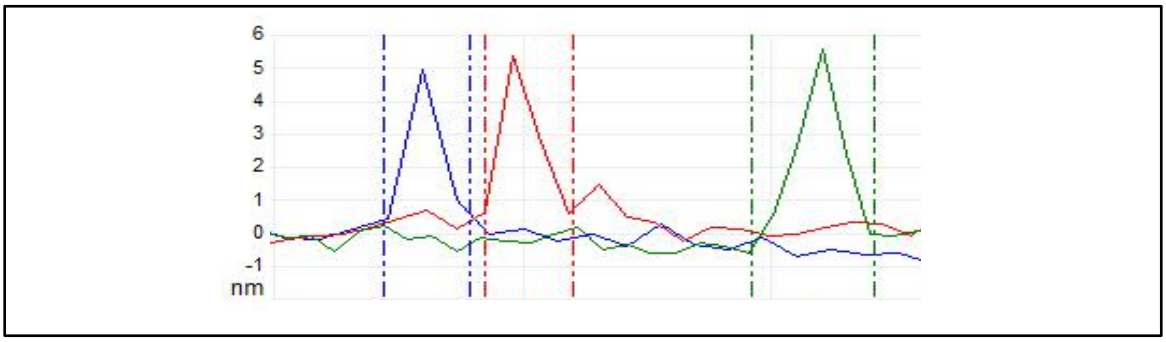

Figure 12 – Three individual particles were selected from the Sup35NM C-terminal His-tag following 5 seconds sonication sample scan (Figure 11b) and analysed using sectioning tool in Bruker Nanoscope Analysis Software to reveal heights between 5 and 6 nm.

3.3.3 Sup35NM C-terminal His-tag fibrils maintained height following extreme sonication.

The Sup35NM C-terminal His-tag fibrils behaved largely as expected after 60 seconds sonication. Visually, small, round 'dots' could be seen and there was a slight variation in size between particles (Figure 13a). When compared to other sonication periods in the series, the height distribution was typical and had a mean of 5.7 nm. This suggested Sup35NM C-terminal His-tag fibrils had a structural stability equivalent to that of the Sup35NM N-terminal His-tag fibrils conventionally used. As expected, the length of the Sup35NM C-terminal His-tag fibrils was reduced significantly following 60 seconds sonication to a mean of 52.8 nm.

Following 240 seconds sonication, the Sup35NM C-terminal His-tag particles were homogenous (Figure 13b). In these images, similar to images of Sup35NM N-terminal His-tag particles, incredibly short fragments were seen. The Sup35NM C-terminal His-tag particles had an average length of 56.4 nm but nevertheless maintained a height of 5.3 nm, this was indicative of a mechanical strength that was much the same as Sup35NM N-terminal His-tag particles.

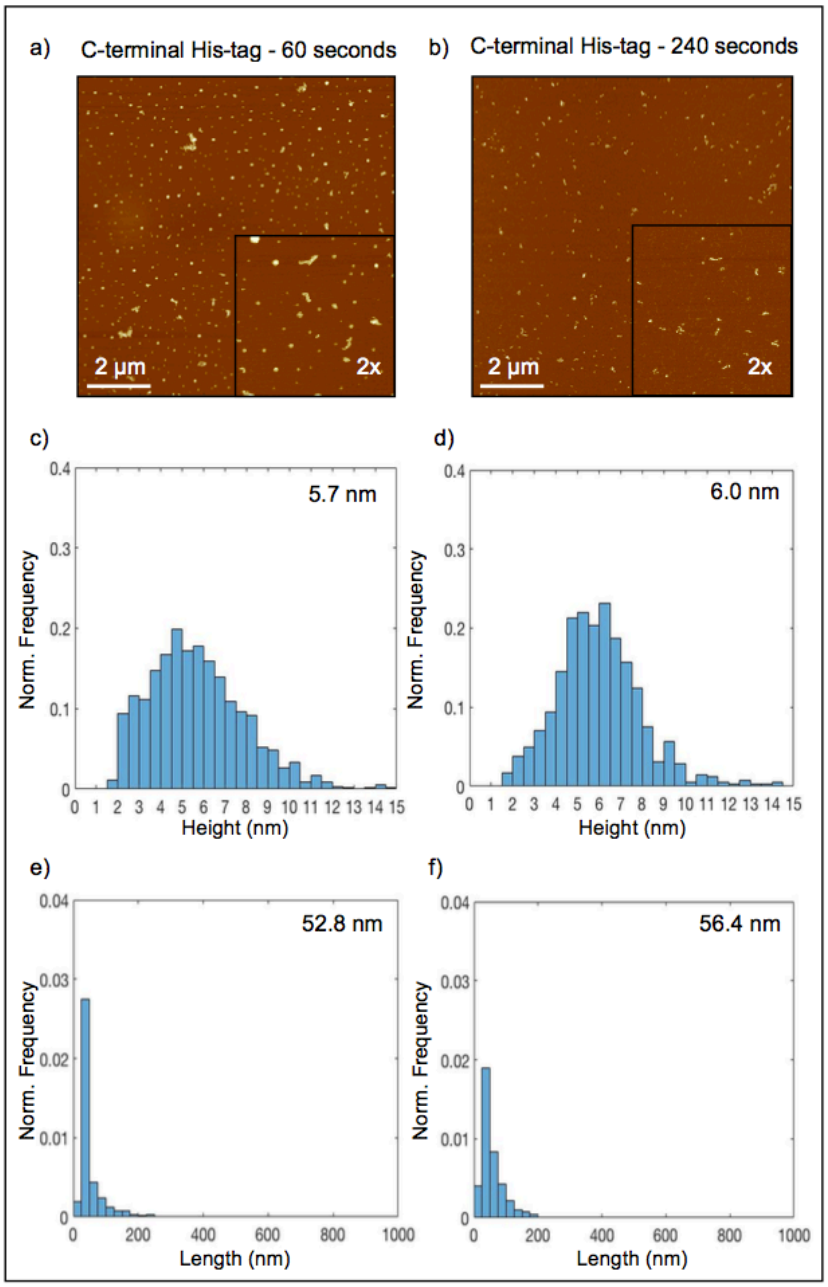

Figure 13 - AFM image of Sup35NM C-terminal His-tag fibrils 0.2 µM following a) 60 seconds b) 240 seconds sonication on mica. Scan size 10x10 µm 1024 x 1024 pixels, and scale bar represents 2 µm for both images. Images collected by N.Koloteva-Levine. Normalised particle height (nm) distribution of Sup35NM C-terminal His-tag fibrils following c) 60 seconds d) 240 seconds sonication. Normalised particle length (nm) distribution of Sup35NM C- terminal His-tag fibrils following e) 60 seconds f) 240 seconds sonication. Mean value displayed in the top right.

3.3.4 Sup35NM C-terminal His-tag fibrils and Sup35NM N-terminal His-tag fibrils were similar.

Overall, it could be said that the Sup35NM C-terminal His-tag fibrils and Sup35NM N-terminal His-tag fibrils were mostly alike and reacted to sonication in a similar fashion, demonstrating they had the same mechanical strength.

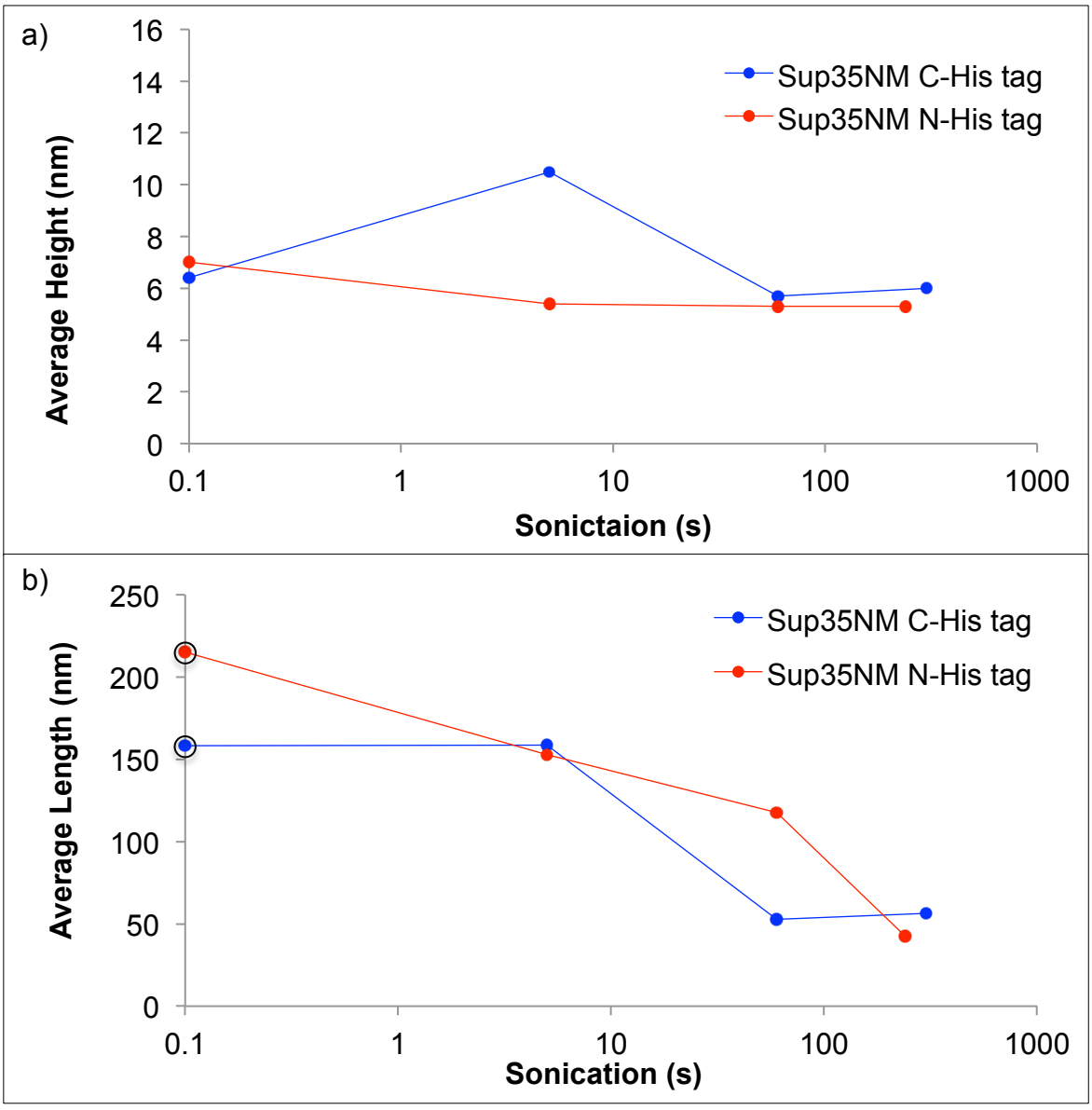

Figure 14 - a) Consistent average height (nm) and b) decreasing average length (nm) of Sup35NM N-terminal His-tag and C-terminal His-tag particles following 0, 5 and 240/300 seconds sonication. Sonication time shown on a logarithmic scale. Values circled to signify fibrils extend outside the scanned area, and thus the value is an underestimation.

Sonication (seconds)	Protein	Average Height (nm)	Average Length (nm)
0	Sup35NM C-His tag	6.4	(>>158.1)
	Sup35NM N-His tag	7.0	(>>215.2)
5	Sup35NM C-His tag	10.5	158.5
	Sup35NM N-His tag	5.4	152.7
60	Sup35NM C-His tag	5.7	52.8
	Sup35NM N-His tag	6.5	117.6
240	Sup35NM C-His tag	6.0	56.4
300	Sup35NM N-His tag	5.3	42.7

Table 2 – Mean height and length data for Sup35NM C-terminal His-tag and Sup35NM N-terminal His-tag, following 0, 5, 60, 240 and 300 seconds sonication. *Notation (>> X) used to signify fibrils extend outside the scanned area, and thus the value is an underestimation.*

Following this investigation, the structure and mechanical stability of Sup35NM and 3 Sup35NM mutants with single substitution mutation in a region identified as vital for prion formation were explored. Specifically, the effect of a change in structure on prion propagation ability was assessed.

3.4 Comparison Of Sup35NM WT And Mutant fibrils

In order to identify what aspects of structure and stability are critical for prion propagation, the factors already identified as affecting propagation in nature must be considered. It has been demonstrated that Sup35NM with a single amino acid residue substitution (G58D) in the OPR region still forms prions, but the mutation impedes prion propagation. Mutants of Sup35NM: G58A, G58K and G58V have been previously assessed for their ability to propagate in colonies, but it remains unknown what structural underpinnings facilitate these varying abilities. This thesis investigated if there was a visual distinction on a mesoscopic scale between mutant and wild type Sup35NM, and progressed to compare the mechanical stability of the mutants through controlled sonication to see if the features affecting prion transmissibility could be elucidated.

3.4.1 The structure of Sup35NM G58A fibrils were not severely affected by the mutation.

The Sup35NM G58A fibrils (Figure 14a) were almost ‘knotted’ in appearance, which was not consistent with the Sup35NM WT fibrils, which overlapped but were still clearly discrete. Despite this ‘knotted’ appearance, the fibrils were long, with a mean length of 141.8 nm. The lack of fragmentation and a height of 6.5 nm, which was consistent with other fibrils under the same conditions, suggested the structure of the G58A variant had not been severely affected by the mutation.

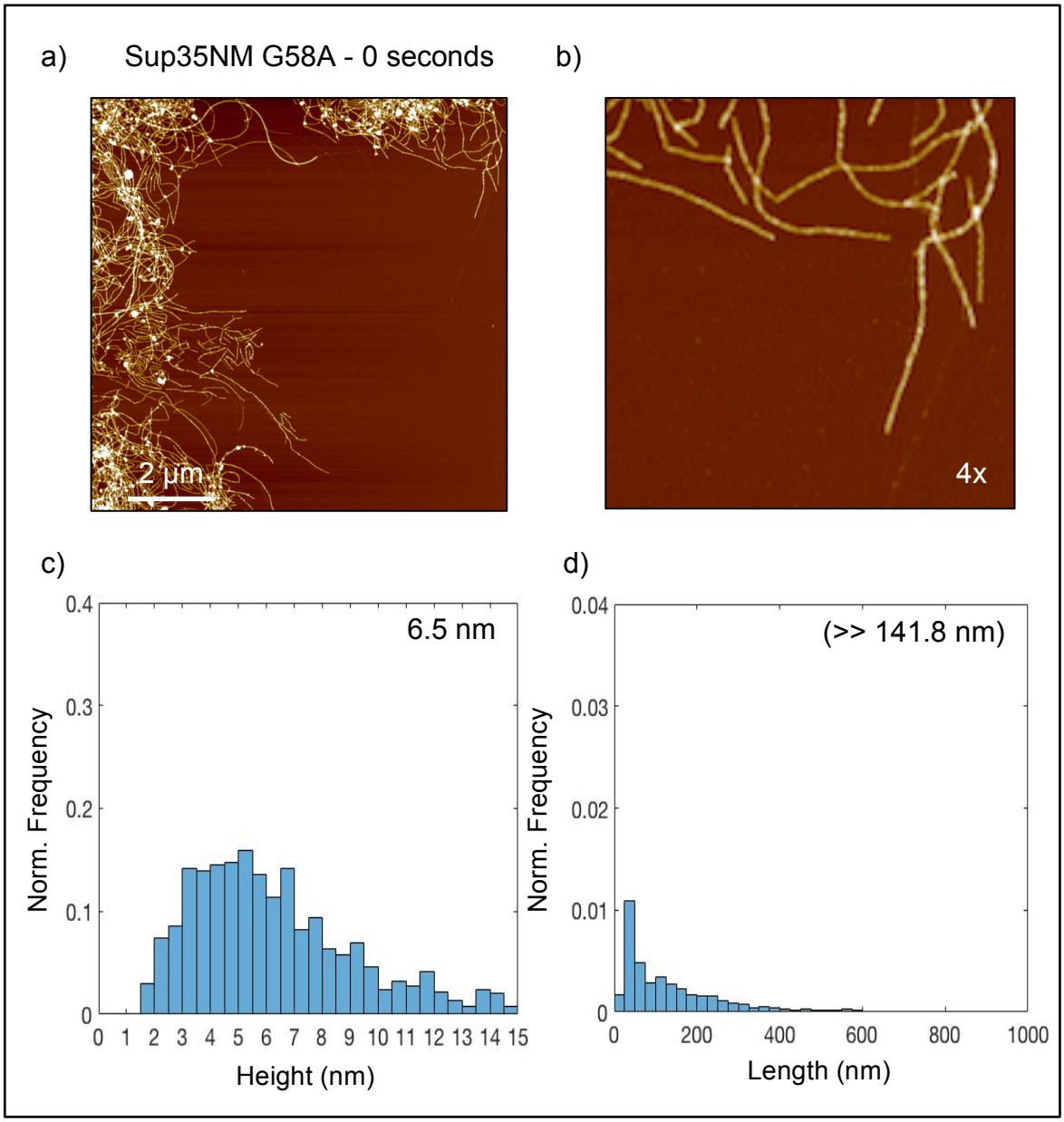

Figure 15 – *Sup35NM G58A fibrils are whole and long, similar to the WT fibrils.* a) *AFM image of unsonicated Sup35NM G58A fibrils (2 µM) following on mica. Scan size 10x10 µm 1024 x 1024 pixels, and scale bar represents 2 µm.* b) *4x magnification.* c) *Normalised particle height (nm) distribution of Sup35NM G58A fibrils.* d) *Normalised particle length (nm) distribution of Sup35NM G58A fibrils. Mean value displayed in the top right. Notation (>> X nm) used to signify fibrils extend outside the scanned area, and thus the value is an underestimation.*

3.4.2 The structure of Sup35NM G58K fibrils were affected considerably by the mutation.

The sample of Sup35NM G58K fibrils contained short clumped fragmented fibrils, highlighted in the 4x magnified view (Figure 16b). The unsonicated fragments bore a closer resemblance to a sample that had been sonicated for 5 seconds or longer. The structure of the fibrils had been considerably affected by the mutation. The mean height of the G58K fibrils was 9.3 nm, seemingly large when compared to an average Sup3NM WT fibril, but presumed to be a reflection of the clumping seen, rather than actual fibril height.

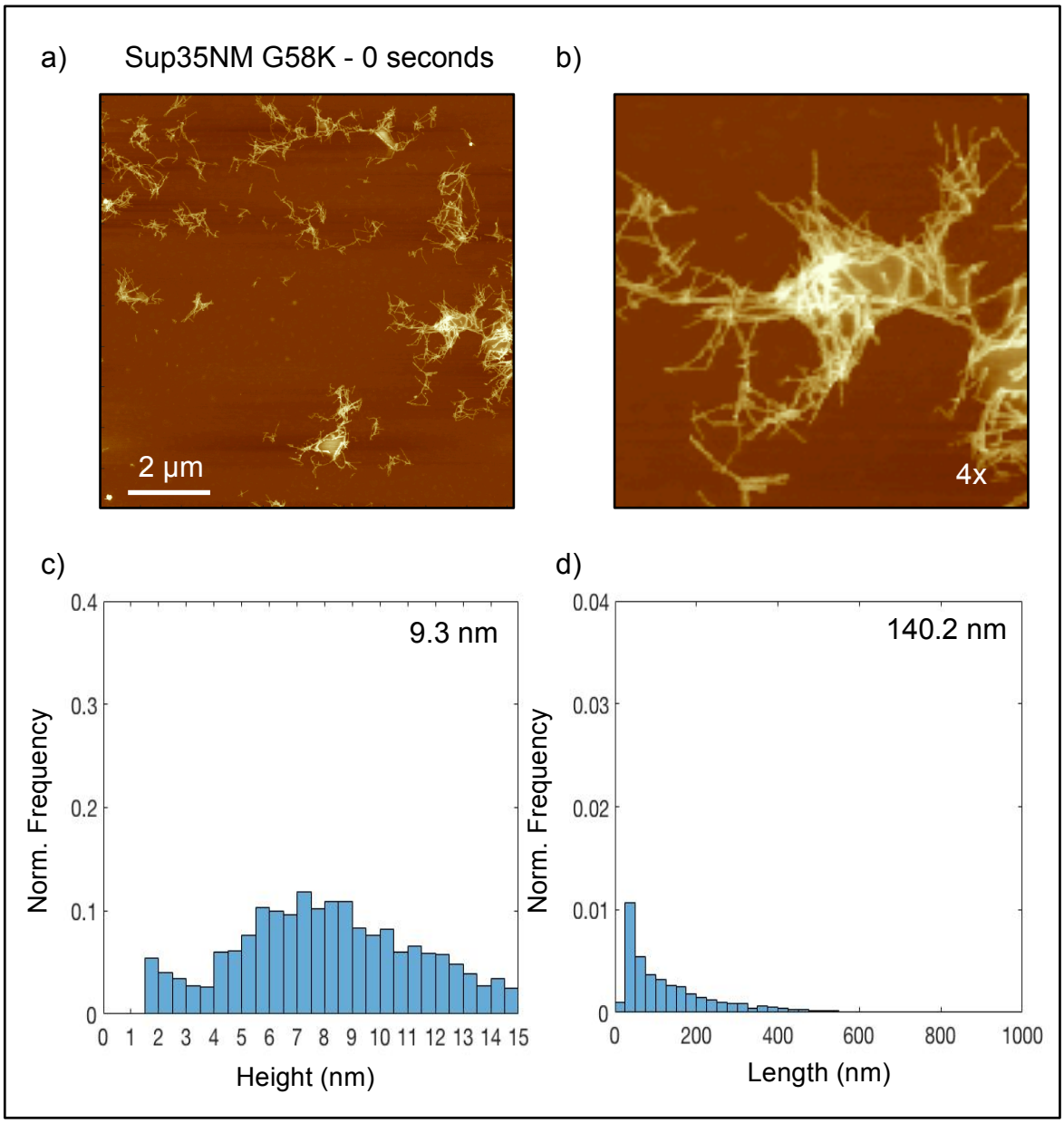

Figure 16 - Sup35NM G58K fibrils fragment without any sonication. a) AFM image of unsonicated Sup35NM G58K fibrils (2 µM) on mica. Scan size 10x10 µm 1024 x 1024 pixels, and scale bar represents 2 µm. b) 4x magnification. c) Normalised particle height (nm) distribution of Sup35NM G58K fibrils. d) Normalised particle length (nm) distribution of Sup35NM G58K fibrils. Mean value displayed in the top right.

3.4.3 Sup35NM G58V fibrils were arguably the closest in appearance to the Sup35NM WT fibrils.

The Sup35NM G58V fibrils (Figure 17) were long, straight and distinct; they were arguably the closest in appearance to the Sup35NM WT fibrils as there was no visible fragmentation in this sample. Sup35NM G58V fibrils also exhibited a distribution of height and length most comparable to Sup35NM WT fibrils. The mean height of the Sup35NM G58V fibrils was 4.9 nm, certainly smaller than the 7.0 nm recorded for the Sup35NM WT fibrils, but both are were the range expected. Sup35NM G58V fibrils also displayed the greatest mean length of all the mutants at 175.2 nm. As clarified previously, any average fibril length recorded prior to sonication was not strictly accurate as fibrils extended outside of the scan area, but a high average length compared to other fibrils was a result of minimal fragmentation.

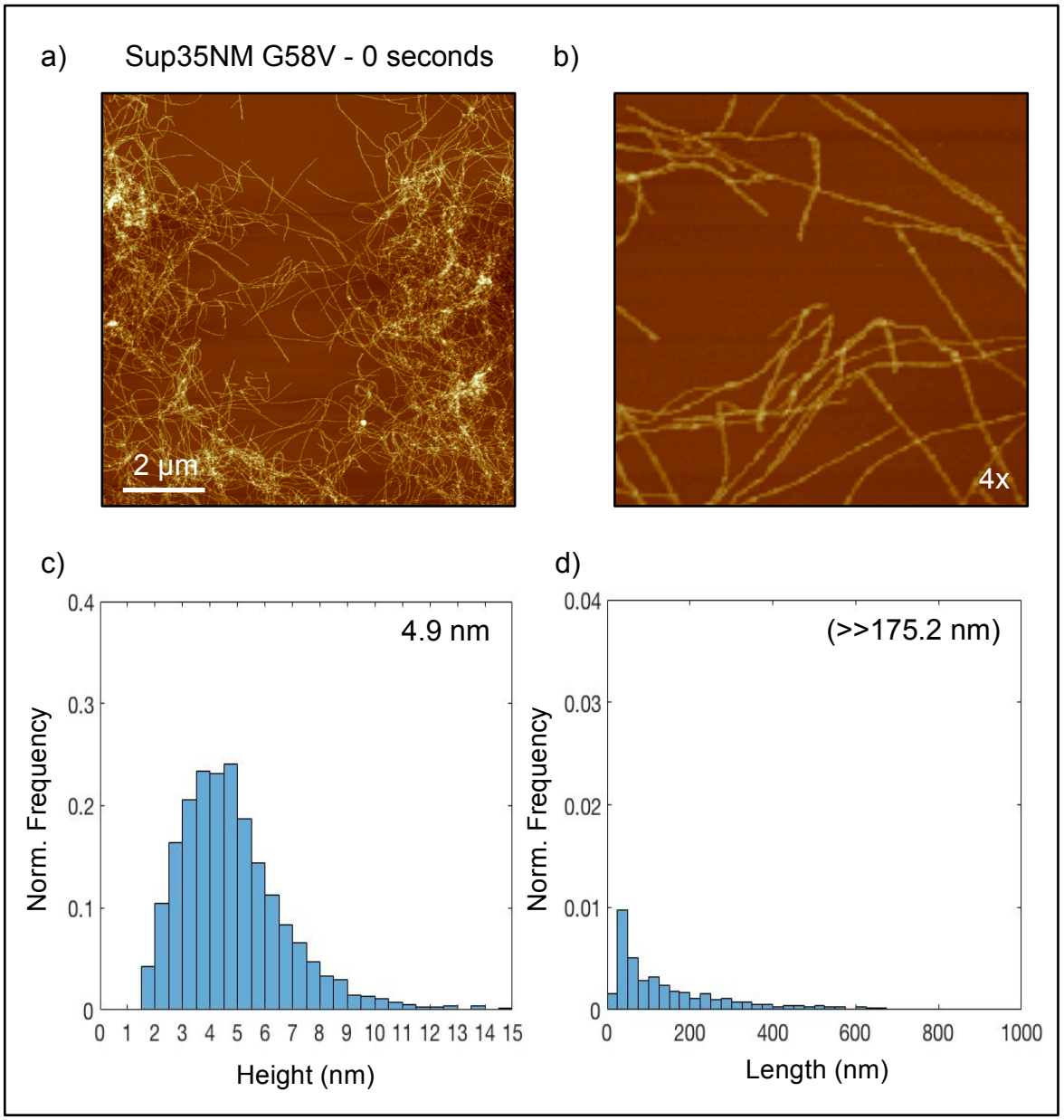

Figure 17 - Sup35NM G58V fibrils are most similar to the WT. a) AFM image of unsonicated Sup35NM G58V fibrils (2 µM) on mica. Scan size 10x10 µm 1024 x 1024 pixels, and scale bar represents 2 µm. b) 4x magnification. c) Normalised particle height (nm) distribution of Sup35NM G58V fibrils. d) Normalised particle length (nm) distribution of Sup35NM G58V fibrils. Mean value displayed in top right. Notation (>> X nm) used to signify fibrils extend outside the scanned area, and thus the value is an underestimation.

3.4.4 Comparison of Sup35NM mutant fibrils with the WT.

Protein	Average Height (nm)	Average Length (nm)
$A\beta_{42}$	6.3	(>>146.3)
Sup35NM WT	7.0	(>>215.2)
Sup35NM G58A	6.5	(>>141.8)
Sup35NM G58K	9.3	140.2
Sup35NM G58V	4.9	(>>175.2)

Table 3 - Mean fibril height and length data for $A\beta_{42}$, Sup35NM WT and Sup35NM mutants: G58A, G58K and G58V. Notation (>> X) used to signify fibrils extend outside the scanned area, and thus the value is an underestimation.

3.4.5 Sup35NM G58K fibrils recorded average height was a reflection of clumping.

The mean height of the G58K fibrils was recorded as 9.3 nm, seemingly large when compared to an average Sup3NM WT fibril. This was later confirmed by single fibril analysis (shown below) to be a reflection of the clumping seen, rather than actual fibril height.

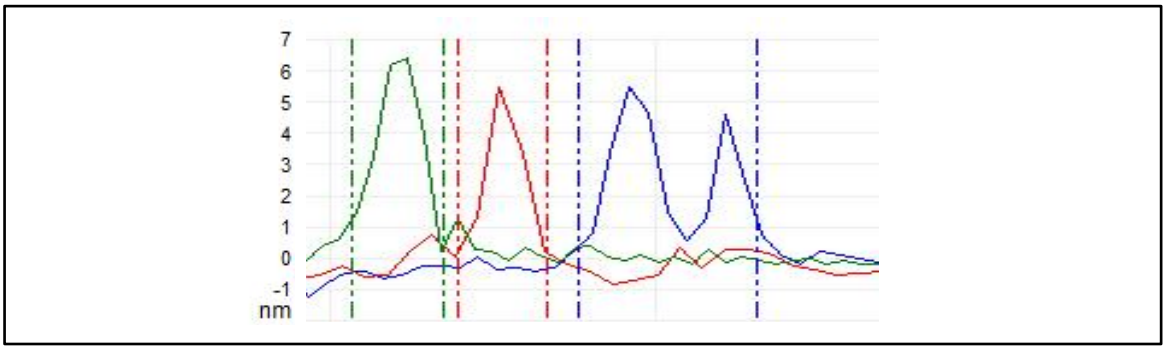

Figure 18 - Four individual particles were selected from the Sup35NM G58K sample scan (Figure 16b) and analysed using sectioning tool in Bruker Nanoscope Analysis Software to reveal heights between 4.5 and 6.2 nm.

After recording and assessing the features of these novel mutant fibrils in their native state, the mutant fibrils were subjected to controlled sonication, to see the extent to which the mutant fibrils tolerated mechanical stress in comparison with the Sup35NM WT fibrils.

It was anticipated that an amino acid substitution would affect the rate of fragmentation and offer an explanation for the variation in the extent of propagation. If proved correct the AA position could be used as a therapeutic target to prevent fragmentation and therefore spread, or at least, a greater understanding of the mechanism of spread in amyloid disease.

3.5 Sup35NM G58A and G58V fibrils were sonicated to assess mechanical stability.

The Sup35NM fibrils with G58A and G58V single amino acid substitutions were selected for further sonication, as these produced the fibrils that were most similar in height, length and overall appearance to the Sup35NM WT fibrils. The Sup35NM G58K sample was omitted at this stage, as the fibrils already resembled sonicated fibrils. The Sup35NM G58A and Sup35NM G58V fibrils were sonicated for a period of 5 seconds with the expectation that, resembling Sup35NM WT and $A\beta_{42}$ samples, the result would be short but whole fibril fragments that sustain height.

3.5.1 Sup35NM G58A fibrils had low mechanical strength.

The Sup35NM G58A fibrils did not react as anticipated to sonication, the fragments appeared non-uniform, thin and clumped (Figure 19a). The fibrils had an average length of approximately half that of the Sup35NM WT at 77.2 nm following 5 seconds sonication. Interestingly, despite the abnormal appearance of the fibrils, fibril height was maintained with a mean height of 4.7 nm. Taking into consideration only the height and length data seen in the histograms the Sup35NM G58A fibrils misleadingly seemed consistent with the sonicated Sup35NM WT fibril data, but on a mesoscopic scale the mutant did not react to mechanical stress as the Sup35NM WT fibrils did. This suggests the fibrils were less mechanically stable, possibly enabling propagation through increased fragmentation.

3.5.2 Sup35NM G58V fibrils had high mechanical strength.

The sonicated Sup35NM G58V fibrils (Figure 19b) bore a closer resemblance to the sonicated Sup35NM WT fibrils than the sonicated Sup35NM G58A fibrils.

Both Sup35NM WT fibrils and Sup35NM G58V fibrils formed short, distinct and whole fragments. The two proteins did differ in that there were more ‘clumps’ of fragments present in the sonicated Sup35NM G58V scan, this was reflected in the deceptive ‘increase’ in height from 4.9 nm in the unsonicated sample, to 8.7 nm at 5 seconds sonication. Nevertheless, the sonicated Sup35NM G58V fibrils had a mean length of 110.3 nm, most analogous to Sup35NM WT at 152.7 nm. The high mechanical strength of the fibrils reduced fragmentation, which in turn possibly negatively affected the rate of propagation.

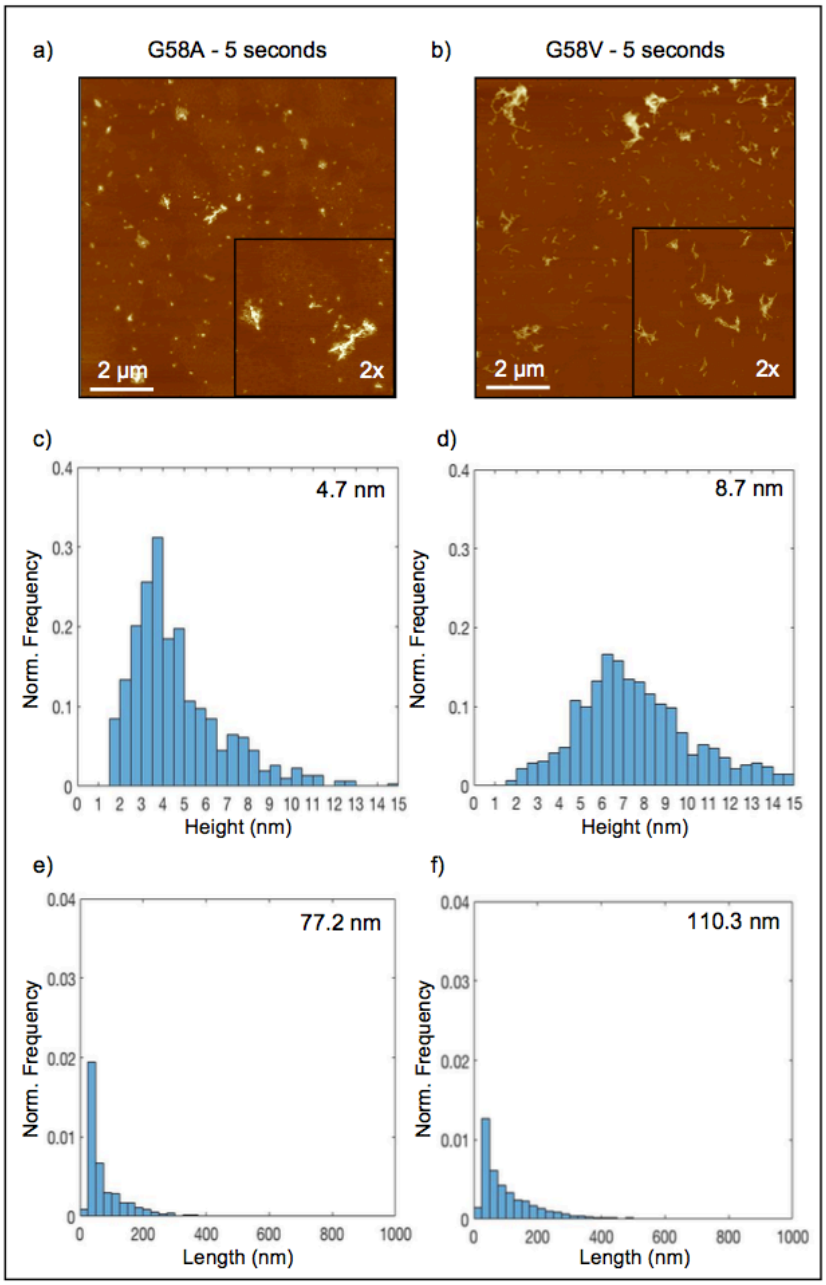

Figure 19 - a) AFM image of Sup35NM G58A particles (0.2 µM) following 5 seconds sonication on mica. b) AFM image of Sup35NM G58V particles (0.2 µM) following 5 seconds sonication on mica. Scan size 10x10 µm 1024 x 1024 pixels, and scale bar represents 2 µm for both images. Normalised particle height (nm) distribution of c) Sup35NM G58A particles d) Sup35NM G58V particles. Normalised particle length (nm) distribution of e) Sup35NM G58A particles f) Sup35NM G58V particles. Mean value displayed in top right.

3.5.3 Analysis of Sup35NM G58A and Sup35NM G58V following sonication.

Protein	Average Height (nm)	Average Length (nm)
$A\beta_{42}$	5.5	131.5
Sup35NM WT	5.4	152.7
Sup35NM G58A	4.7	77.2
Sup35NM G58V	8.7	110.3

Table 4 – Mean height and length data for $A\beta_{42}$, Sup35NM WT and Sup35NM mutants G58A and G58V, following 5 seconds sonication.

Bringing together the results of the unsonicated mutant fibrils and the results in this experiment following sonication, it was clear that Sup35NM G58V fibrils most closely resembled the Sup35 WT fibrils, both visually in AFM scans and when comparing average height and length data. G58A fibrils were less mechanically stable than the WT along the length of the fibril, possibly enabling greater fragmentation and more propagation.

4. DISCUSSION

4.1 A comparison of $A\beta_{42}$ and Sup35NM fibrils.

Sup35 is a protein found in *Saccharomyces cerevisiae*, in nature this protein is a eukaryotic translation release factor (eRF3) (Volkov *et al.*, 2007). In cells with the [*PSI*+] phenotype Sup35 is in a prion state, meaning it exists as an amyloid and can propagate to daughter cells (Cox, 1965; Krammer *et al.*, 2009). In order to propagate the prion must maintain height to enable it to be a template for replication, physically act as a nucleus seed or 'starting block' to recruit and convert soluble proteins for new fibril growth (Ohhashi *et al.*, 2010). Flow field-flow fractionation has been used to separate prions by size and has confirmed that oligomers composed of 14–28 monomers exhibit the most infection properties *in vivo* (Silveira *et al.*, 2005).

The molecular and structural basis behind the creation and spread of prions is poorly understood (Grant, 2015). It is known that all prions have an amyloid structure and amyloid proteins share this common cross β sheet structure regardless of the precursor protein (Nelson *et al.*, 2005). As such Sup35 is often used as a model to explore the qualities of disease-associated proteins such as $A\beta_{42}$. Sup35 is an epigenetic regulator of cell physiology and has the advantage of being non-cytotoxic, allowing its characteristics and mechanisms to be investigated without killing the host cell (Xu, Bevis and Arnsdorf, 2001; Kryndushkin *et al.*, 2002; Osherovich *et al.*, 2004).

The question remains, how analogous is the structure and structural stability of these two proteins on a mesoscopic scale? Furthermore, could any disparity explain the difference in infectious potential between the two amyloid? Does

easier fragmentation (enabled by low mechanical stability) allow for greater propagation? In order to maintain core structural integrity as they fragmented, both proteins were expected to be capable of sustaining height under simulated mechanical force in the form of controlled sonication. Sup35NM and $A\beta_{42}$ fibrils were sonicated at 3 time points to assess their mechanical strength and the extent to which disease-associated mammalian prions and model yeast prions were consistent.

4.1.1 Disparity between unsonicated $A\beta_{42}$ and Sup35NM fibrils.

Interestingly, before sonication there was already a minor disparity between the appearance of $A\beta_{42}$ and Sup35NM fibrils. The $A\beta_{42}$ fibrils appeared somewhat fragmented in comparison to the long Sup35NM fibrils that could be traced uninterrupted from one side of the scan to the other. This initial assessment was reinforced by the height and length data collected by AFM, which reported an average length of 146.3 nm for $A\beta_{42}$ and a much longer length of 215.2 nm for Sup35NM. Lengths were not accurate prior to sonication as fibrils extended out of the scan area; however, the significantly smaller average length of $A\beta_{42}$ was most likely the result of a greater proportion of shorter fragments. This variation in fibril appearance and dimension was attributed to the different roles of the proteins.

Sup35 has a role in translation and as such the concentration of available Sup35 fluctuates in the cell according to need. In nature, Sup35 proteostasis and prion spread are controlled by a complicated and not yet fully understood system of chaperone proteins. One of which, HSP104, a homohexameric AAA ATPase, is responsible for the creation of small prion particles or ‘seeds’ that are able to leave the cell *in vivo* (Chernoff *et al.*, 1995; Paushkin *et al.*, 1996). It follows that recombinant Sup35NM fibrils would be less prone to fragment in the absence of

these chaperone proteins. HSP104 is specific to Sup35 and has no homologue in mammalian cells (Krauss and Vorberg, 2013). Mammalian cells do contain disaggregates that could be considered orthologs, which act unspecifically to break down plaques, creating toxic oligomers. It would follow that $A\beta_{42}$ is more liable to fragment (than Sup35), independent of cellular machinery, due to intrinsic low mechanical stability along the length of the $A\beta_{42}$ fibril. $A\beta_{42}$ is a disease-associated protein; its pathogenic role is by virtue of particle spread. The tendency to fragment uncontrollably and without assistance is an asset in a prion/prion-like protein with a pathogenic role, as it would lead to an even greater proportion of small toxic oligomers.

4.1.2 Sonication revealed the mechanical strength of $A\beta_{42}$ and Sup35NM fibrils.

Following 5 and 300 seconds sonication the two proteins were near indistinguishable at the same time point, in regards to both suprastructure and recorded height and length data. Strikingly, all sonicated samples maintained height between the narrow range of 5 to 7 nm. This demonstrated the incredible mechanical strength across the height of the fibrils, a testament to the importance of maintaining height to prion/prion-like protein propagation.

4.2 The effect of protein purification tags on Sup35NM.

Polyhistidine affinity tags (His-tags) have been used for decades to efficiently purify large quantities of protein. The gene sequence of the desired protein is altered to add six or more consecutive histidine residues at the C- or N- terminus. The His-tag in the desired protein binds to immobilised metal cations in a column and (once separated from impurities) is eluted. His-tags are small and were widely considered to have no effect on the structure or function of the protein, indeed one of their greatest benefits. However, recently papers have been published with evidence to suggest that His-tags and their location may interfere with protein aggregation, activity and structure (Goel *et al.*, 2000; Carson *et al.*, 2007; Sayari *et al.*, 2007; Thielges *et al.*, 2011; Majorek *et al.*, 2014).

To investigate this possibility further, Sup35NM fibrils with a C-terminal His-tag were produced, scanned, and sonicated to assess the mechanical stability of the fibrils. These results were compared to the Sup35NM fibrils with an N-terminal His-tag, which is the variant conventionally used in Sup35NM investigation. Any significant variation in results between the Sup35NM fibrils with a C-terminal His-tag and an N-terminal His-tag would suggest that the His-tag had a detrimental effect on Sup35NM structure or activity.

4.2.1 Sup35NM C-terminal and N-terminal His-tag fibrils were visually alike.

The unsonicated C-terminal His-tag fibrils were compared with their N-terminal His-tag equivalents. At first glance, the C-terminal His-tag fibrils appear whole long and distinct, very similar in appearance to the more commonly used N-terminal His-tag Sup35NM. This initial assessment is supported by the height and length data gathered from analysis by AFM, which recorded an average fibril

height of 6.4 nm and an average length of 158.1 nm for C-terminal His-tag fibrils, both values in the range expected.

4.2.2 Sup35NM C-terminal and N-terminal His-tag fibrils had near identical mechanical strength.

The fibrils were sonicated over 3 different time points to assess their mechanical stability. Mechanical stability should ideally be identical between the two fibrils. Thus, similar to the Sup35NM fibrils with an N-terminal His-tag, it was expected that the Sup35NM fibrils with a C-terminal His-tag would maintain height as length decreased with each increasing sonication time.

Following 5 seconds sonication the fibrils did not appear as expected. It appeared as though fragmented fibrils of an expected length were created but unfortunately, the fibrils formed amorphous aggregates. A possible explanation is that the protein sample may have been left too long before plating. Nonetheless, discrete particles outside the body of clumping had normal fibril height dimensions between 5 and 7 nm when individually analysed by sectioning tools on Nanoscope software.

Following an even longer duration of sonication for 60 and 300 seconds the Sup35NM fibrils with a C-terminal His-tag not only maintained a height and length comparable to that of the Sup35NM fibrils with an N-terminal His-tag but additionally maintained height throughout all sonication periods, suggesting that both fibrils had incredible mechanical stability perpendicular to the axis of the fibril. Importantly, both fibrils appeared and responded the same to perturbation by controlled sonication. As a result of these observations, it is apparent that the presence and placement of a His-tag bears no significant effect on Sup35NM

suprastructure or mechanical stability, further endorsing previous work done with the N-terminal His-tag Sup35NM in the investigation of prion/prion-like proteins.

Although it has been found that the placement of His-tag does not have a detrimental effect on the suprastructure or mechanical stability of Sup35NM in isolation, it could interfere with its interaction with chaperone proteins such as HSP104, which enable prion propagation, an interesting possibility to investigate in the future.

4.3. The impact of site-directed mutagenesis on the structure, stability and prion propagation of Sup35NM mutants.

It is known that a single amino acid substitution has the potential to impact the stability and propagation of a prion. This has been investigated and reported in prions such as the mammalian prion PrP^{sc}, in which a naturally occurring variant (with a valine residue at position 129 instead of a methionine residue) can act to prevent the development of Creutzfeldt-Jakob disease by influencing the folding and oligomerisation of the protein (Palmer *et al.*, 1991; Tahiri-Alaoui *et al.*, 2004).

In yeast cells, the phenotype [*PSI*$^{+}$] signifies that the translation termination factor Sup35 is in its propagating prion form. There is a Sup35 mutant named PNM for "[*PSI*$^{+}$] no more" which is a functional protein with a typical amyloid structure that is able to enter prion aggregates but acts to reduce the spread of the [*PSI*$^{+}$] phenotype. PNM has a single amino acid substitution (G58D) in the OPR domain of Sup35, a domain that has been highlighted as nonessential for viability or translation termination but crucial for prion propagation (Ter-Avanesyan *et al.*, 1994; Kochneva-Pervukhova *et al.*, 1998; Verges *et al.*, 2011).

In a previous study by Marchante and colleagues *(Marchante et al., 2013b)* site-directed mutagenesis was used to create a comprehensive collection of Sup35NM G58X mutants, which were later selected for on a medium containing 5FOA (5-Fluoroorotic Acid). This phenotypic assay indicated with a colour change the percent of induced [*PSI*$^{+}$] colonies for each mutant and thus revealed how capable each mutant was of prion propagation (Cox and Tuite, 2018). One mutant from each class was selected for further analysis. They found that the G58A mutant was one of the most phenotypically stable mutants, as the percent of induced [*PSI*$^{+}$] colonies was comparable to that of the wild type. The G58K

mutant was less phenotypically stable, with only some induction of [*PSI*$^{+}$] and the G58V mutant was highly unstable leading to very little induction of [*PSI*$^{+}$] (Marchante *et al.*, 2013b). Our scan images and height-length data analysis largely supported these findings for the G58A and G58K Sup35NM mutants, but held unexpected results for the Sup35NM G58V mutant.

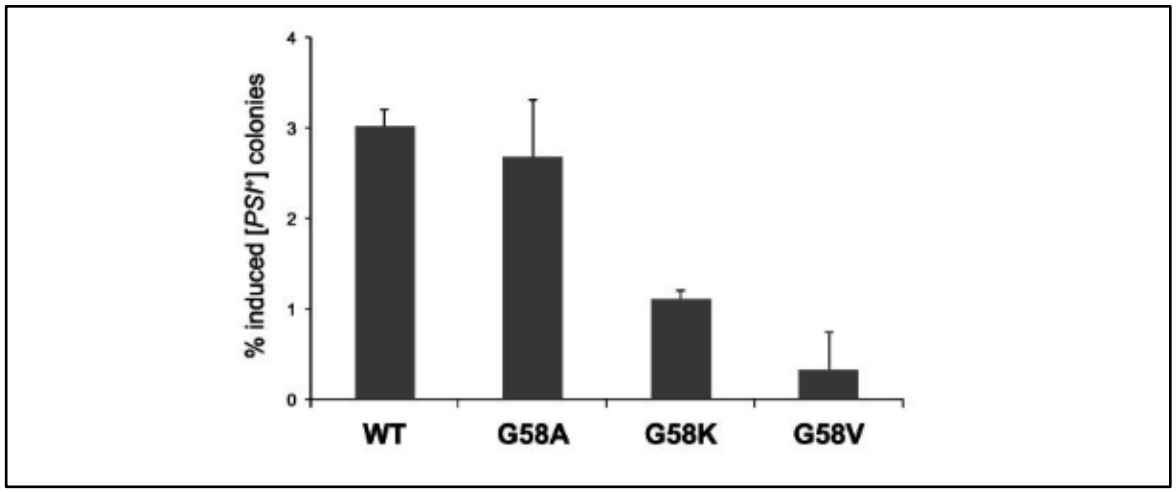

Figure 20 – *Percent of induced* [*PSI*+] *colonies for Sup35NM wild type and three G58X mutants, assessed by scoring the number of* [*PSI*+] *colonies in a phenotypic assay. The G58A variant induced the* [*PSI*+] *phenotype at a similar frequency as the wild type. G58K variant induced less* [*PSI*+] *colonies, and the G58V variant induced very few. Adapted from: (Marchante et al., 2013b).*

4.3.1 The structure of the Sup35NM G58A mutant fibrils were largely unaffected, enabling the mutant to propagate effectively.

The G58A mutant was highlighted as the mutant with the most efficient [*PSI*$^{+}$] propagation in colonies (in some cases more effective than the WT) and as such it was expected to be the most similar in appearance to the wild type. It was concluded that the G58A mutant was similar to the Sup35NM WT in that the Sup35NM G58A mutant fibrils were long and little fragmentation was detected. Furthermore, it was found that of all the mutants the G58A mutant fibrils had the most similar height to the Sup35NM WT fibrils (6.5 nm and 7.0 nm respectively).

The effect of the single point substitution in each mutant is a direct result of the characteristics of the new residue. Alanine is one of the smallest residues; small size is a desirable characteristic in this situation because glycine (the original residue) is the smallest possible amino acid, with a side chain consisting of a single hydrogen atom. It is conceivable that the similarity in size was responsible for the minimal effect of this particular substitution on the structure and therefore the minimal impact on the propagation of this mutant. It is possible that alanine provided a 'weak link' enabling greater fragmentation and propagation.

4.3.2 The structure of the Sup35NM G58K mutant fibrils were drastically affected, negatively impacting prion propagation.

The G58K mutant, which was highlighted as a mutant with intermediate [*PSI*$^{+}$] propagation capability *in vivo*, was the least similar to the Sup35NM WT in appearance, height and length following AFM analysis. The sample appeared broken and clumped, and as a result of overlapping fibril fragments had an average height of 9.3 nm.

Unsurprisingly, lysine, the residue used in this mutant is considerably dissimilar from its small and inert predecessor glycine. Lysine is large, polar and positively charged under biological conditions. Consequently, the mutation had a large adverse impact on structure and propagation.

4.3.3 The structure of the Sup35NM G58V mutant fibrils were unaffected, despite not being capable of effective prion propagation.

The G58V mutant was selected as the least effective at prion propagation following the phenotypic assay. Accordingly, it was expected that the G58V mutant fibrils would reflect this, but remarkably, the fibrils bore the closest

resemblance to the Sup35NM WT. Fibrils were whole, distinct and long with an average length of 175.2 nm, the most similar to the Sup35NM WT sample, which had a mean length of 215.2 nm. The G58V mutant sample was arguably closer in dimension and appearance to the wild type, even more so than the G58A mutant, which was selected as the mutant most effective at propagating in the phenotypic assay (Marchante *et al.*, 2013b). It is conceivable that the G58V fibrils were exceedingly stable, reducing fragmentation and preventing effective propagation.

The conflicting evidence between structure and effect on propagation in colonies suggests the residue in this position is not only responsible for maintaining a suitable structure to enable propagation but additionally contributes specific chemical properties that are vital to fragmentation and the mechanism underpinning prion propagation which are not yet completely understood. This theory would provide rationale for mutants such as G58V and PNM (G58D) that, despite having a conventional structure, fail to propagate adequately and disturb normal function.

4.4 Controlled sonication was used to assess the mechanical stability of Sup35NM WT, G58A And G58V.

Following the analysis of unsonicated Sup35NM WT and mutants, the mechanical stability of G58A and G58V mutants was investigated by subjecting the fibrils to 5 seconds sonication. Previously, it was found that Sup35NM WT particles maintained height, and thus structural integrity despite sonication; this alluded to the importance of the conservation of the height of a fibril to its function as a prion. The conservation of the height despite fragmentation along the length of the fibril was thought to be necessary for the new particles produced to act as templates and nuclei for new fibril growth. The heights and lengths of the selected mutants were recorded following sonication and the impact of sonication on the suprastructure of the mutants was assessed.

4.4.1 Sup35NM G58K was omitted.

The Sup35NM G58K mutant was omitted at this stage. The unsonicated sample already appeared perturbed despite not being subject to sonication yet and therefore offered a clear explanation as to why the mutant could not function as a prion or successfully propagate at the same rate as the wild type in the phenotypic assay, it was simply not structurally stable enough. This further highlights the importance of structure, as without suitable structure there was no effective propagation.

4.4.2 Sup35NM G58A mutant particles did not have the same mechanical strength as the wild type.

As before, the Sup35NM G58A mutant was selected as the mutant with the most efficient [*PSI* $^{+}$] propagation in colonies, accordingly, it was expected to be the most similar to the Sup35NM WT. Despite forming particles of an acceptable

height at 4.7 nm the sonicated Sup35NM G58A particles saw a reduction from the 6.5 nm previously recorded in the unsonicated sample. At 77.2 nm the particles were almost half the length recorded for the wild type under the same conditions, this suggested the mutant had lower mechanical strength than the wild type along the length of the fibril, which allowed it to fragment with greater ease, and thus enabled efficient propagation. However, the mutant particles were not similar in appearance to the wild type particles, the force of sonication had undeniably affected the integrity of the structure of the mutant.

4.4.3 Sup35NM G58V mutant particles continued to be the most analogous to the wild type.

Following 5 seconds sonication the Sup35NM G58V particles, again, behaved most comparable to the Sup35 WT particles. Indeed, the Sup35NM G58V mutant particles appeared more ‘clumped’ than the WT counterpart and consequently had a greater mean height than expected at 8.7 nm, but an average length closer to expectation at 110.3 nm. Despite the initial ‘clumpy’ appearance the particles appeared to have a similar shape and dimensions to the Sup35NM wild type particles.

These findings, combined with the results of the unsonicated mutant samples led to the conclusion that the Sup35NM G58V mutant fibrils appeared and behaved the same as the Sup35NM WT fibrils, yet these similarities did not translate into equal prion propagation ability. This further reinforced the theory proposed earlier: that structure and mechanical stability are prerequisites for effective prion propagation, but far from the only contributing factor. Prions must indeed have a structure that facilitates the physical requirements of prion propagation (to fragment without altering the height, in order to act as a template and nucleus

seed for new fibril growth) but it is also clear that on a molecular level highly specific chemical combinations (in addition to a highly specific structure) are needed in the mechanism for propagation of prions. An extraordinary feat given that prions, despite sharing a common amyloid structure, do not require the same, or even similar, precursor proteins and thus differ significantly in primary sequence and chemical composition.

The intricacies of the mechanisms behind prion seeding, growth and propagation cannot be resolved simply through analysis of structure alone, it must be in combination with investigation into molecular detail and simultaneously the impact *in vivo*. This is not to say that structure is not of vital importance; structure facilitates prion function and how it does will certainly be key to understanding and eventually preventing prion propagation.

4.5 Conclusions

In summary three main conclusions can be drawn following this series of investigations:

Firstly, it was found that Sup35NM and $A\beta_{42}$ fibrils appeared different under native conditions. The pathogenic role of $A\beta_{42}$ is a potential explanation for this disparity, as the more liable a fibril is to fragmentation, the more small toxic particles capable of propagation it will generate, and therefore, the greater its pathogenic potential. Following sonication the two amyloid appeared similar on a mesoscopic scale and importantly had high mechanical strength perpendicular to the fibril axis and low mechanical strength parallel to the fibril axis. This was inferred as both fibrils maintained height irrespective of sonication and fragmented length-wise at a similar rate. The maintenance of height under such force emphasised the importance of height to prion/prion-like protein propagation. Specifically, the height of the fibril is necessary for the integrity of the nucleus or 'seed' required for new fibril growth. It would be interesting to expand this investigation to other Aβ variants such as $A\beta_{40}$ to see if there is a distinction in mechanical stability that underlies the different levels of disease-association between the variants, and eventually, other disease associated prion-like proteins such as Tau.

Secondly, it was confirmed that in the case of Sup35NM the presence and placement of a His-tag did not negatively affect suprastructure or mechanical stability. This control should be a widespread practice where it is not possible or convenient to cleave a purification tag. Our C-terminal and N-terminal His-tag Sup35NM variations proved near identical in suprastructure and mechanical stability, but this is not always the case. Only two criteria have been assessed

here, in the future it would be worthwhile investigating the extent to which purification tags interfere with chaperone binding (such as HSP104) as this would have a significant impact on prion propagation.

Thirdly, it was found that surprisingly, despite being near identical in appearance and mechanical strength to the wild type, Sup35NM G58V mutant, much like the Sup35NM G58D mutant fibrils, did not propagate efficiently *in vivo*. This suggests that although structure is a necessary prerequisite for effective prion propagation it is not the only contributing factor. Although undoubtedly structure has a part to play in enabling prion and prion-like protein propagation, the reduced mechanical stability appears to have had the greatest impact on propagation by increasing the ease of fragmentation and the creation of more oligomers. Further investigation on a molecular level is needed to elucidate the specific mechanism behind propagation. While it is anticipated amino acid position 58 will have a large role to play the fragmentation mechanism, it is not yet know what triggers fragmentation, or how.

Overall, considering amyloid structure on a mesoscopic level, understanding its mechanical stability, and how these features facilitate the mechanism behind prion/prion-like propagation will be vital in the fight against debilitating conditions such as Alzheimer's disease. The lack of progress thus far in finding an effective treatment is undoubtedly a result of a lack of focus on structural and molecular detail and failure to take these into account when designing pharmaceuticals. Studies like these, which combine *in vivo* data with detail on a mesoscopic level, are crucial. Elucidating the mechanism behind prion propagation and importantly, how structure enables it, will be key to one day finding a cure.

5. REFERENCES

Abbott, A. (2016) ‘The red-hot debate about transmissible Alzheimer’s.’, *Nature*, 531(7594), pp. 294–7.

Allison, D. P. *et al.* (2010) ‘Atomic force microscopy of biological samples.’, *Wiley interdisciplinary reviews. Nanomedicine and nanobiotechnology*, 2(6), pp. 618–34.

Alzheimer’s Association (2016) ‘2016 Alzheimer’s disease facts and figures.’, *Alzheimer’s & dementia : the journal of the Alzheimer’s Association*, 12(4), pp. 459–509.

Andréoletti, O. *et al.* (2012) ‘Highly Efficient Prion Transmission by Blood Transfusion’, *PLoS Pathogens*. Edited by J. Bartz, 8(6), p.e1002782.

Annus, Á., Csáti, A. and Vécsei, L. (2016) ‘Prion diseases: New considerations.’, *Clinical neurology and neurosurgery*, 150, pp. 125–132.

Antzutkin, O. N. *et al.* (2002) ‘Supramolecular Structural Constraints on Alzheimer’s β-Amyloid Fibrils from Electron Microscopy and Solid-State Nuclear Magnetic Resonance’, *Biochemistry*, 41(51), pp. 15436–15450.

Appleby, B. S. *et al.* (2013) ‘Iatrogenic Creutzfeldt-Jakob disease from commercial cadaveric human growth hormone.’, *Emerging infectious diseases*. Centers for Disease Control and Prevention, 19(4), pp. 682–4.

Balbirnie, M., Grothe, R. and Eisenberg, D. S. (2001) ‘An amyloid-forming peptide from the yeast prion Sup35 reveals a dehydrated beta-sheet structure for amyloid.’, *Proceedings of the National Academy of Sciences of the United States of America*, 98(5), pp. 2375–80.

Biancalana, M., Makabe, K. and Koide, S. (2010) ‘Minimalist design of water-soluble cross-beta architecture.’, *Proceedings of the National Academy of Sciences of the United States of America*, 107(8), pp. 3469–74.

Blennow, K., de Leon, M. J. and Zetterberg, H. (2006) 'Alzheimer's disease.', *Lancet (London, England)*, 368(9533), pp. 387–403.

Bolduc, D. M. *et al.* (2016) 'The amyloid-beta forming tripeptide cleavage mechanism of γ-secretase.', *eLife*, 5. pp. 17578.

Bond, M. *et al.* (2012) 'The effectiveness and cost-effectiveness of donepezil, galantamine, rivastigmine and memantine for the treatment of Alzheimer's disease (review of Technology Appraisal No. 111): a systematic review and economic model.', *Health technology assessment (Winchester, England)*, 16(21), pp. 1–470.

Bondarev, S. A. *et al.* (2014) 'Modification of [PSI+] prion properties by the combination of amino acid changes within Sup35 protein N-domain.', *Molekuliarnaia biologiia*, 48(2), pp. 314–21.

Brion, J. P. (1998) 'Neurofibrillary tangles and Alzheimer's disease.', *European neurology*, 40(3), pp. 130–40.

Carson, M. *et al.* (2007) 'His-tag impact on structure.', *Acta crystallographica. Section D, Biological crystallography*, 63(Pt 3), pp. 295–301.

Chatani, E. and Yamamoto, N. (2018) 'Recent progress on understanding the mechanisms of amyloid nucleation.', *Biophysical reviews*, 10(2), pp. 527–534.

Chernoff, Y. O. *et al.* (1995) 'Role of the chaperone protein Hsp104 in propagation of the yeast prion-like factor [psi+].', *Science (New York, N.Y.)*, 268(5212), pp. 880–4.

Cohen, S. I. A. *et al.* (2013) 'Proliferation of amyloid-β42 aggregates occurs through a secondary nucleation mechanism.', *Proceedings of the National Academy of Sciences of the United States of America*, 110(24), pp. 9758–63.

Colby, D. W. and Prusiner, S. B. (2011) 'Prions.', *Cold Spring Harbor perspectives in biology*, 3(1), p. a006833.

Cox, B. S. (1965) 'Ψ, A cytoplasmic suppressor of super-suppressor in yeast',

Heredity. Nature Publishing Group, 20(4), pp. 505–521.

Cox, B. and Tuite, M. (2018) 'The life of [PSI].', *Current genetics*. Springer, 64(1), pp. 1–8.

Cremades, N. *et al.* (2012) 'Direct observation of the interconversion of normal and toxic forms of α-synuclein.', *Cell*, 149(5), pp. 1048–59.

Cutlip, R. C. *et al.* (1994) 'Intracerebral transmission of scrapie to cattle.', *The Journal of infectious diseases*, 169(4), pp. 814–20.

Das, A. S. and Zou, W.-Q. (2016) 'Prions: Beyond a Single Protein', *Clinical Microbiology Reviews*, 29(3), pp. 633–658.

Diack, A. B. *et al.* (2014) 'Variant CJD. 18 years of research and surveillance.', *Prion*. Taylor & Francis, 8(4), pp. 286–95.

Diaz-Avalos, R. *et al.* (2003) 'Cross-beta order and diversity in nanocrystals of an amyloid-forming peptide.', *Journal of molecular biology*, 330(5), pp. 1165–75.

Diaz-Espinoza, R. and Soto, C. (2010) 'Generation of prions in vitro and the protein-only hypothesis.', *Prion*. Taylor & Francis, 4(2), pp. 53–9.

Dubois, B. *et al.* (2016) 'Timely Diagnosis for Alzheimer's Disease: A Literature Review on Benefits and Challenges.', *Journal of Alzheimer's disease : JAD*. IOS Press, 49(3), pp. 617–31.

Fraser, P. E. (2014) 'Prions and prion-like proteins.', *The Journal of biological chemistry*, 289(29), pp. 19839–40.

Frid, P., Anisimov, S. V and Popovic, N. (2007) 'Congo red and protein aggregation in neurodegenerative diseases.', *Brain research reviews*, 53(1), pp. 135–60.

Goel, A. *et al.* (2000) 'Relative position of the hexahistidine tag effects binding properties of a tumor-associated single-chain Fv construct.', *Biochimica et biophysica acta*, 1523(1), pp. 13–20.

Grant, C. M. (2015) 'Sup35 methionine oxidation is a trigger for de novo [PSI(+)]

prion formation.', *Prion*, 9(4), pp. 257–65.

Gu, L. and Guo, Z. (2013) 'Alzheimer's Aβ42 and Aβ40 peptides form interlaced amyloid fibrils', *Journal of Neurochemistry*, 126(3), pp. 305–311.

Hauw, J.-J., Haik, S. and Brandel, J.-P. (2015) 'History of Prions and transmission of protein misfolding.', *Bulletin de l'Academie nationale de medecine*, 199(6), pp. 787–796.

Hellstrand, E. *et al.* (2010) 'Amyloid β-protein aggregation produces highly reproducible kinetic data and occurs by a two-phase process.', *ACS chemical neuroscience*. American Chemical Society, 1(1), pp. 13–8.

Ironside, J. W., Ritchie, D. L. and Head, M. W. (2017) 'Prion diseases.', *Handbook of clinical neurology*, 145, pp. 393–403.

Jahn, T. R. *et al.* (2010) 'The common architecture of cross-beta amyloid.', *Journal of molecular biology*, 395(4), pp. 717–27.

Jensen, E. (2013) 'Types of imaging, Part 3: Atomic force microscopy.', *Anatomical record (Hoboken, N.J. : 2007)*, 296(2), pp. 179–83.

Kashchiev, D. (2015) 'Protein Polymerization into Fibrils from the Viewpoint of Nucleation Theory.', *Biophysical journal*, 109(10), pp. 2126–36.

Kayed, R. and Lasagna-Reeves, C. A. (2012) 'Molecular Mechanisms of Amyloid Oligomers Toxicity', *Journal of Alzheimer's Disease*. Edited by G. Perry et al., 33(s1), pp. S67–S78.

Kochneva-Pervukhova, N. V *et al.* (1998) 'Mechanism of inhibition of Psi+ prion determinant propagation by a mutation of the N-terminus of the yeast Sup35 protein.', *The EMBO journal*, 17(19), pp. 5805–10.

Krammer, C. *et al.* (2009) 'The yeast Sup35NM domain propagates as a prion in mammalian cells.', *Proceedings of the National Academy of Sciences of the United States of America*, 106(2), pp. 462–7.

Kraus, A., Groveman, B. R. and Caughey, B. (2013) 'Prions and the Potential

Transmissibility of Protein Misfolding Diseases', *Annual Review of Microbiology*, 67(1), pp. 543–564.

Krauss, S. and Vorberg, I. (2013) 'Prions Ex Vivo: What Cell Culture Models Tell Us about Infectious Proteins.', *International journal of cell biology*, 2013, pp. 704546.

Kryndushkin, D. S. *et al.* (2002) 'Increased expression of Hsp40 chaperones, transcriptional factors, and ribosomal protein Rpp0 can cure yeast prions.', *The Journal of biological chemistry*, 277(26), pp. 23702–8.

Kumar, A., Singh, A. and Ekavali (2015) 'A review on Alzheimer's disease pathophysiology and its management: an update.', *Pharmacological reports : PR*, 67(2), pp. 195–203.

Kumar, P. *et al.* (2015) 'Tau phosphorylation, molecular chaperones, and ubiquitin E3 ligase: clinical relevance in Alzheimer's disease.', *Journal of Alzheimer's disease : JAD*, 43(2), pp. 341–61.

Lee, G. and Leugers, C. J. (2012) 'Tau and tauopathies.', *Progress in molecular biology and translational science*, 107, pp. 263–93.

Liberski, P. P. (2012) 'Historical overview of prion diseases: a view from afar.', *Folia neuropathologica*, 50(1), pp. 1–12.

Lieschke, G. J. and Currie, P. D. (2007) 'Animal models of human disease: zebrafish swim into view.', *Nature reviews. Genetics*, 8(5), pp. 353–67.

Ma, J. and Wang, F. (2014) 'Prion disease and the "protein-only hypothesis".', *Essays in biochemistry*, 56, pp. 181–91.

MacKenzie, C. *et al.* (2002) 'Transmission of prion diseases by blood transfusion', *Journal of General Virology*, 83(11), pp. 2897–2905.

Madine, J. *et al.* (2008) 'Structural insights into the polymorphism of amyloid-like fibrils formed by region 20-29 of amylin revealed by solid-state NMR and X-ray fiber diffraction.', *Journal of the American Chemical Society*, 130(45), pp. 14990–

5001.

Majorek, K. A. *et al.* (2014) ‘Double trouble-Buffer selection and His-tag presence may be responsible for nonreproducibility of biomedical experiments.’, *Protein science : a publication of the Protein Society*. Wiley-Blackwell, 23(10), pp. 1359–68.

Mangialasche, F. *et al.* (2010) ‘Alzheimer’s disease: clinical trials and drug development.’, *The Lancet. Neurology*, 9(7), pp. 702–16.

Marchante, R. *et al.* (2013a) ‘Structural definition is important for the propagation of the yeast [PSI+] prion.’, *Molecular cell*, 50(5), pp. 675–85.

Marchante, R. *et al.* (2013b) ‘Structural definition is important for the propagation of the yeast [PSI+] prion.’, *Molecular cell*, 50(5), pp. 675–85.

Marchante, R. *et al.* (2017) ‘The physical dimensions of amyloid aggregates control their infective potential as prion particles.’, *eLife*. eLife Sciences Publications, pp. 6.

Marešová, P. *et al.* (2015) ‘Socio-economic Aspects of Alzheimer’s Disease.’, *Current Alzheimer research*, 12(9), pp. 903–11.

Marešová, P., Klímová, B. and Kuča, K. (2015) ‘Alzheimers disease: cost cuts call for novel drugs development and national strategy.’, *Ceska a Slovenska farmacie : casopis Ceske farmaceuticke spolecnosti a Slovenske farmaceuticke spolecnosti*, 64(1–2), pp. 25–30.

Marshall, K. E. *et al.* (2014) ‘The relationship between amyloid structure and cytotoxicity.’, *Prion*, 8(2).

Marshall, K. E. and Serpell, L. C. (2009) ‘Structural integrity of β-sheet assembly’, *Biochemical Society Transactions*, 37(4), pp. 671–676.

Mathiason, C. K. (2017) ‘Scrapie, CWD, and Transmissible Mink Encephalopathy.’, *Progress in molecular biology and translational science*, 150, pp. 267–292.

McCarthy, M. (2013) ‘Cost of dementia care in US to double by 2040.’, *BMJ (Clinical research ed.)*, 346, p. f2175.

McCutcheon, S. *et al.* (2011) ‘All clinically-relevant blood components transmit prion disease following a single blood transfusion: a sheep model of vCJD.’, *PloS one*. Public Library of Science, 6(8), p. e23169.

Moore, R. A., Faris, R. and Priola, S. A. (2015) ‘Proteomics applications in prion biology and structure.’, *Expert review of proteomics*, 12(2), pp. 171–84.

Morkvėnaitė-Vilkončienė, I., Ramanavičienė, A. and Ramanavičius, A. (2013) ‘Atomic force microscopy as a tool for the investigation of living cells.’, *Medicina (Kaunas, Lithuania)*, 49(4), pp. 155–64.

Morris, K. L. and Serpell, L. C. (2012) ‘X-ray fibre diffraction studies of amyloid fibrils.’, *Methods in molecular biology (Clifton, N.J.)*, 849, pp. 121–35.

Nelson, R. *et al.* (2005) ‘Structure of the cross-beta spine of amyloid-like fibrils.’, *Nature*, 435(7043), pp. 773–8.

Nelson, R. and Eisenberg, D. (2006a) ‘Recent atomic models of amyloid fibril structure.’, *Current opinion in structural biology*, 16(2), pp. 260–5.

Nelson, R. and Eisenberg, D. (2006b) ‘Structural models of amyloid-like fibrils.’, *Advances in protein chemistry*, 73, pp. 235–82.

Ohhashi, Y. *et al.* (2010) ‘Differences in prion strain conformations result from non-native interactions in a nucleus.’, *Nature chemical biology*, 6(3), pp. 225–230.

Ono, K., Condron, M. M. and Teplow, D. B. (2009) ‘Structure-neurotoxicity relationships of amyloid beta-protein oligomers.’, *Proceedings of the National Academy of Sciences of the United States of America*, 106(35), pp. 14745–50.

Osherovich, L. Z. *et al.* (2004) ‘Dissection and design of yeast prions.’, *PLoS biology*. Edited by Greg Petsko, 2(4), pp. E86.

de Pablo, P. J. and Carrión-Vázquez, M. (2014) ‘Imaging biological samples with

atomic force microscopy.', *Cold Spring Harbor protocols*, 2014(2), pp. 167–77.

Palmer, M. S. *et al.* (1991) 'Homozygous prion protein genotype predisposes to sporadic Creutzfeldt-Jakob disease.', *Nature*, 352(6333), pp. 340–2.

Panza, F. *et al.* (2014) 'Is there still any hope for amyloid-based immunotherapy for Alzheimer's disease?', *Current opinion in psychiatry*, 27(2), pp. 128–37.

Parham, S. N., Resende, C. G. and Tuite, M. F. (2001) 'Oligopeptide repeats in the yeast protein Sup35p stabilize intermolecular prion interactions', *The EMBO Journal*, 20(9), pp. 2111–2119.

Paushkin, S. V *et al.* (1996) 'Propagation of the yeast prion-like [psi+] determinant is mediated by oligomerization of the SUP35-encoded polypeptide chain release factor.', *The EMBO journal*, 15(12), pp. 3127–34.

Pham, C. L. L., Kwan, A. H. and Sunde, M. (2014) 'Functional amyloid: widespread in Nature, diverse in purpose', *Essays In Biochemistry*, 56, pp. 207–219.

Pouryamout, L. *et al.* (2012) 'Economic evaluation of treatment options in patients with Alzheimer's disease: a systematic review of cost-effectiveness analyses.', *Drugs*, 72(6), pp. 789–802.

Prusiner, S. B. (1982) 'Novel proteinaceous infectious particles cause scrapie.', *Science (New York, N.Y.)*, 216(4542), pp. 136–44.

Rajamohamedsait, H. B. and Sigurdsson, E. M. (2012) 'Histological staining of amyloid and pre-amyloid peptides and proteins in mouse tissue.', *Methods in molecular biology (Clifton, N.J.)*, 849, pp. 411–24.

Rambaran, R. N. and Serpell, L. C. (2008) 'Amyloid fibrils: abnormal protein assembly.', *Prion*. Taylor & Francis, 2(3), pp. 112–7.

Sakono, M. and Zako, T. (2010) 'Amyloid oligomers: formation and toxicity of Aβ oligomers', *FEBS Journal*, 277(6), pp. 1348–1358.

Sawaya, M. R. *et al.* (2007) 'Atomic structures of amyloid cross-beta spines

reveal varied steric zippers.', *Nature*, 447(7143), pp. 453–7.

Sayari, A. *et al.* (2007) 'The N-terminal His-tag affects the enantioselectivity of staphylococcal lipases: a monolayer study.', *Journal of colloid and interface science*, 313(1), pp. 261–7.

Seed, C. R. *et al.* (2018) 'Creutzfeldt-Jakob disease and blood transfusion safety.', *Vox sanguinis*, 113(3), pp. 220–231.

Serafini, G. *et al.* (2016) 'Suicide Risk in Alzheimer's Disease: A Systematic Review.', *Current Alzheimer research*, 13(10), pp. 1083–99.

Serpell, L. C. (2000) 'Alzheimer's amyloid fibrils: structure and assembly.', *Biochimica et biophysica acta*, 1502(1), pp. 16–30.

Serpell, L. C., Sunde, M. and Blake, C. C. (1997) 'The molecular basis of amyloidosis.', *Cellular and molecular life sciences : CMLS*, 53(11–12), pp. 871–87.

Shanthi, K. B., Krishnan, S. and Rani, P. (2015) 'A systematic review and meta-analysis of plasma amyloid 1-42 and tau as biomarkers for Alzheimer's disease.', *SAGE open medicine*. SAGE Publications, 3, pp. 1-9.

Sibener, L. *et al.* (2014) 'Alzheimer's Disease prevalence, costs, and prevention for military personnel and veterans.', *Alzheimer's & dementia : the journal of the Alzheimer's Association*, 10(3 Suppl), pp. 105-10.

Silveira, J. R. *et al.* (2005) 'The most infectious prion protein particles.', *Nature*, 437(7056), pp. 257–61.

Sipe, J. D. and Cohen, A. S. (2000) 'Review: history of the amyloid fibril.', *Journal of structural biology*, 130(2–3), pp. 88–98.

Soto, C. and Castilla, J. (2004) 'The controversial protein-only hypothesis of prion propagation.', *Nature medicine*, 10 Suppl(7), pp. S63-7.

Stromer, T. and Serpell, L. C. (2005) 'Structure and morphology of the Alzheimer's amyloid fibril.', *Microscopy research and technique*, 67(3–4), pp.

210–7.

Stroud, J. C. *et al.* (2012) ‘Toxic fibrillar oligomers of amyloid-β have cross-β structure.’, *Proceedings of the National Academy of Sciences of the United States of America*, 109(20), pp. 7717–22.

Sunde, M. *et al.* (1997) ‘Common core structure of amyloid fibrils by synchrotron X-ray diffraction.’, *Journal of molecular biology*, 273(3), pp. 729–39.

Tahiri-Alaoui, A. *et al.* (2004) ‘Methionine 129 Variant of Human Prion Protein Oligomerizes More Rapidly than the Valine 129 Variant’, *Journal of Biological Chemistry*, 279(30), pp. 31390–31397.

Ter-Avanesyan, M. D. *et al.* (1994) ‘The SUP35 omnipotent suppressor gene is involved in the maintenance of the non-Mendelian determinant [psi+] in the yeast Saccharomyces cerevisiae.’, *Genetics*, 137(3), pp. 671–6.

Thielges, M. C. *et al.* (2011) ‘Influence of histidine tag attachment on picosecond protein dynamics.’, *Biochemistry*, 50(25), pp. 5799–805.

Tuite, M. F. (2000) ‘Yeast prions and their prion-forming domain.’, *Cell*, 100(3), pp. 289–92.

Tycko, R. (2000) ‘Solid-state NMR as a probe of amyloid fibril structure.’, *Current opinion in chemical biology*, 4(5), pp. 500–6.

Tycko, R. (2006) ‘Molecular structure of amyloid fibrils: insights from solid-state NMR.’, *Quarterly reviews of biophysics*, 39(1), pp. 1–55.

Tycko, R. and Wickner, R. B. (2013) ‘Molecular structures of amyloid and prion fibrils: consensus versus controversy.’, *Accounts of chemical research*, 46(7), pp. 1487–96.

Ushiki, T. (2001) ‘Atomic force microscopy and its related techniques in biomedicine.’, *Italian journal of anatomy and embryology = Archivio italiano di anatomia ed embriologia*, 106(2 Suppl 1), pp. 3–8.

Uversky, V. N. and Lyubchenko, Y. (2013) '*Bio-Nanoimaging : Protein Misfolding*

& Aggregation'., Academic Press, pp 1-552.

Vahabi, S., Nazemi Salman, B. and Javanmard, A. (2013) 'Atomic force microscopy application in biological research: a review study.', *Iranian journal of medical sciences*, 38(2), pp. 76–83.

Verdile, G. *et al.* (2004) 'The role of beta amyloid in Alzheimer's disease: still a cause of everything or the only one who got caught?', *Pharmacological research*, 50(4), pp. 397–409.

Verges, K. J. *et al.* (2011) 'Strain conformation, primary structure and the propagation of the yeast prion [PSI+].', *Nature structural & molecular biology*, 18(4), pp. 493–9.

Voisin, T. and Vellas, B. (2009) 'Diagnosis and treatment of patients with severe Alzheimer's disease.', *Drugs & aging*, 26(2), pp. 135–44.

Volkov, K. *et al.* (2007) 'N-terminal extension of *Saccharomyces cerevisiae* translation termination factor eRF3 influences the suppression efficiency of *sup35* mutations', *FEMS Yeast Research*, 7(3), pp. 357–365.

Wickner, R. B. *et al.* (2015) 'Yeast prions: structure, biology, and prion-handling systems.', *Microbiology and molecular biology reviews : MMBR*, 79(1), pp. 1–17.

Wogulis, M. *et al.* (2005) 'Nucleation-dependent polymerization is an essential component of amyloid-mediated neuronal cell death.', *The Journal of neuroscience : the official journal of the Society for Neuroscience*, 25(5), pp. 1071–80.

Xu, S. (2009) 'Cross-beta-sheet structure in amyloid fiber formation.', *The journal of physical chemistry. B*, 113(37), pp. 12447–55.

Xu, S., Bevis, B. and Arnsdorf, M. F. (2001) 'The assembly of amyloidogenic yeast sup35 as assessed by scanning (atomic) force microscopy: an analogy to linear colloidal aggregation?', *Biophysical journal*, 81(1), pp. 446–54.

Xue, W.-F. *et al.* (2009) 'Fibril fragmentation enhances amyloid cytotoxicity.', *The*

Journal of biological chemistry. American Society for Biochemistry and Molecular Biology, 284(49), pp. 34272–82.

Xue, W.-F. *et al.* (2010) 'Fibril fragmentation in amyloid assembly and cytotoxicity: when size matters.', *Prion*, 4(1), pp. 20–5.

Xue, W.-F. (2015) 'Nucleation: The Birth of a New Protein Phase.', *Biophysical journal*, 109(10), pp. 1999–2000.

Xue, W.-F., Homans, S. W. and Radford, S. E. (2008) 'Systematic analysis of nucleation-dependent polymerization reveals new insights into the mechanism of amyloid self-assembly.', *Proceedings of the National Academy of Sciences of the United States of America*, 105(26), pp. 8926–31.

Xue, W.-F., Homans, S. W. and Radford, S. E. (2009) 'Amyloid fibril length distribution quantified by atomic force microscopy single-particle image analysis.', *Protein engineering, design & selection : PEDS*, 22(8), pp. 489–96.

Xue, W.-F. and Radford, S. E. (2013) 'An imaging and systems modeling approach to fibril breakage enables prediction of amyloid behavior.', *Biophysical journal*, 105(12), pp. 2811–9.

Zabel, M. D. and Reid, C. (2015) 'A brief history of prions.', *Pathogens and disease*. Edited by P. Bavoil, 73(9), pp. 87.

Zhang, Z., Nie, S. and Chen, L. (2018) 'Targeting prion-like protein spreading in neurodegenerative diseases', *Neural Regeneration Research*, 13(11), p. 1875.

APPENDIX 1 – Thioflavin T Graph

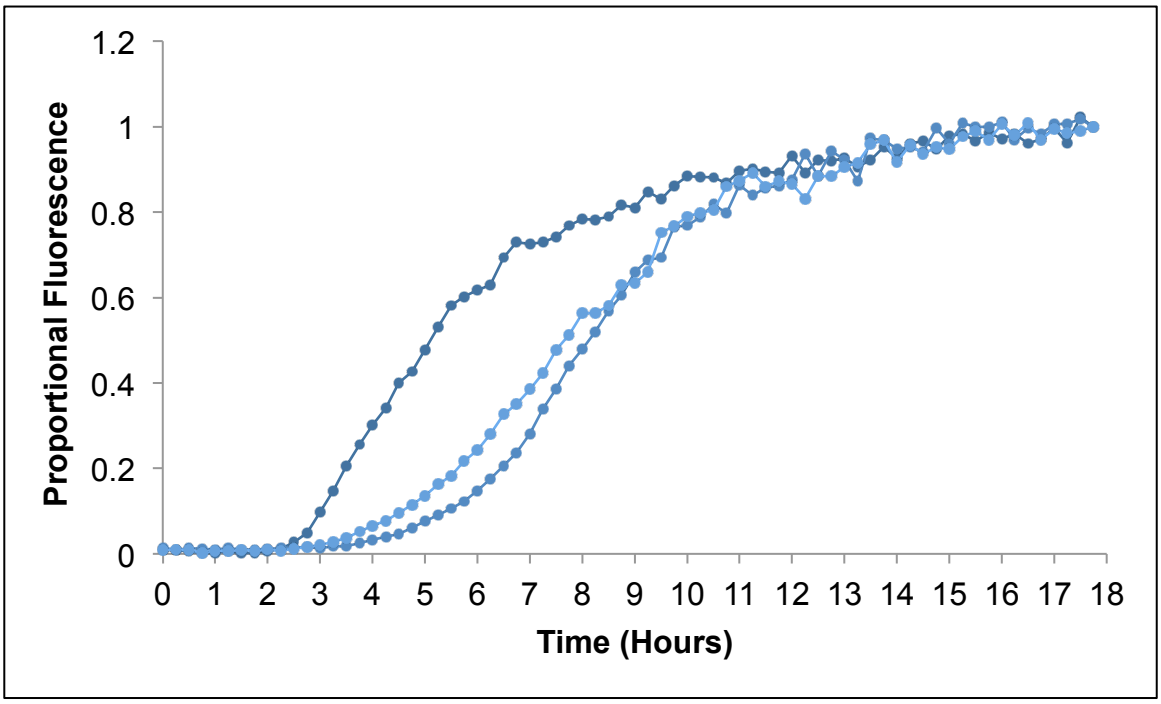

Sup35NM polymerised at 30℃ for 48 hours. For monitoring polymerisation, 3 x 100 µl samples of Sup35NM were aliquoted and Thioflavin T was added to a final concentration of 10 mM. Kinetics were monitored in a FLUOstar OMEGA plate reader (BMG Labtech) at 30℃ until stationary phase reached. The number of hours taken to achieve stationary phases suggests the sample was not contaminated.

APPENDIX 2 - Optimisation Of Fibril Tracing

Noise command line:

```
>> [fitSegments, zresidual, zmodel] = TracePolContour(x, y, z, w, hCutoff);
```

Tracing command line:

```
>> [particles, f] = LinkSegments(fitSegments, width, hCutoff, norm, cutoff, x, y, z);
```

Variable name in Matlab				Comment
width	hCutoff	norm	cutoff	
				512 x 512 pixel crop trialled
5	5			Fibrils selected as noise, try smaller value
2.5	2.5			Noise parameters successful
2	2			Noise parameters also successful
2	2	2	2	Error message, try larger values
2	2	5	5	Traced multiple fibrils as one fibril
2	2	10	10	Some fibrils traced, increase again
2	2	15	20	Most fibrils traced, increase again
2	2	16	20	All fibrils traced accurately
2	2	16	20	Applied to 1024 x 1024 pixel image

The parameters suggested in the methods and materials section were found using this trial and error method exemplified above. The suggested parameters are largely applicable for all the scans. Note that the noise parameters must be accurate before proceeding to the tracing step. Parameters were trialled on a smaller crop first to save processing time.

APPENDIX 3 - Data Summary

Protein	Time (s)	Pixels^2	Resolution	Particle no.	Mean Height (nm)	Height STD (nm)	Height Skewness	Mean Length (nm)	Length STD(nm)	Length Skewness
Aβ42	0	1024	9.8	1864	6.3	2.9	1.0	(146.3)	168.4	2.9
Sup35NM	0	1024	9.8	1516	7.0	1.6	0.1	(215.2)	279.8	3.7
Aβ42	5	1024	9.8	527	5.5	1.6	1.2	131.5	95.3	1.8
Sup35NM	5	1024	9.8	2477	5.4	1.7	3.2	152.7	158.9	2.9
Aβ42	300	1024	9.8	2130	5.7	1.3	0.0	38.5	19.3	3.0
Sup35NM	300	1024	9.8	1950	5.3	2.0	1.2	42.7	34.6	3.4
C-His	0	1024	9.8	3599	6.4	3.2	1.7	(158.1)	156.1	2.0
N-His	0	1024	9.8	1516	7.0	1.6	0.1	(215.2)	279.8	3.7
C-His	5	512	19.5	313	10.5	7.6	0.8	158.5	147.2	1.9
N-His	5	1024	9.8	2477	5.4	1.7	3.2	152.7	158.9	2.9
C-His	60	1024	9.8	1225	5.7	2.2	0.8	52.8	50.5	5.0
N-His	60	1024	9.8	2694	6.5	2.5	8.8	117.6	93.3	2.1
C-His	240	1024	9.8	890	6.0	2.0	1.0	56.4	35.9	1.9
N-His	300	1024	9.8	1950	5.3	2.0	1.2	42.7	34.6	3.4
WT	0	1024	9.8	1516	7.0	1.6	0.1	(215.2)	279.8	3.7
G58A	0	455	9.8	1023	6.5	3.4	1.3	(141.8)	142.5	2.5
G58K	0	1024	9.8	2812	9.3	4.7	1.1	140.2	131.0	2.0
G58V	0	682	9.8	2419	4.9	2.1	1.9	(175.2)	198.6	2.6
WT	5	1024	9.8	2477	5.4	1.7	3.2	152.7	158.9	2.9
G58A	5	1024	9.8	650	4.7	2.2	1.8	77.2	68.2	2.2
G58V	5	1024	9.8	1743	8.7	4.4	1.5	110.3	98.3	1.9

Brief summary of scans collected and data analysed. Abbreviations C-His and N-His refer to C-terminal His-tag Sup35NM and N-terminal His-tag Sup35NM respectively. G58A, G58K, G58V and WT are variants of Sup35NM. Underlined values have been subject to single-particle analysis to confirm average height values are large due to clumping. Notation (X) used to signify fibrils extend outside the scanned area, and thus the value is an underestimation. Standard deviation (STD) values are large as natural variation in particles is large.

APPENDIX 4 - Maintenance Of Particle Height

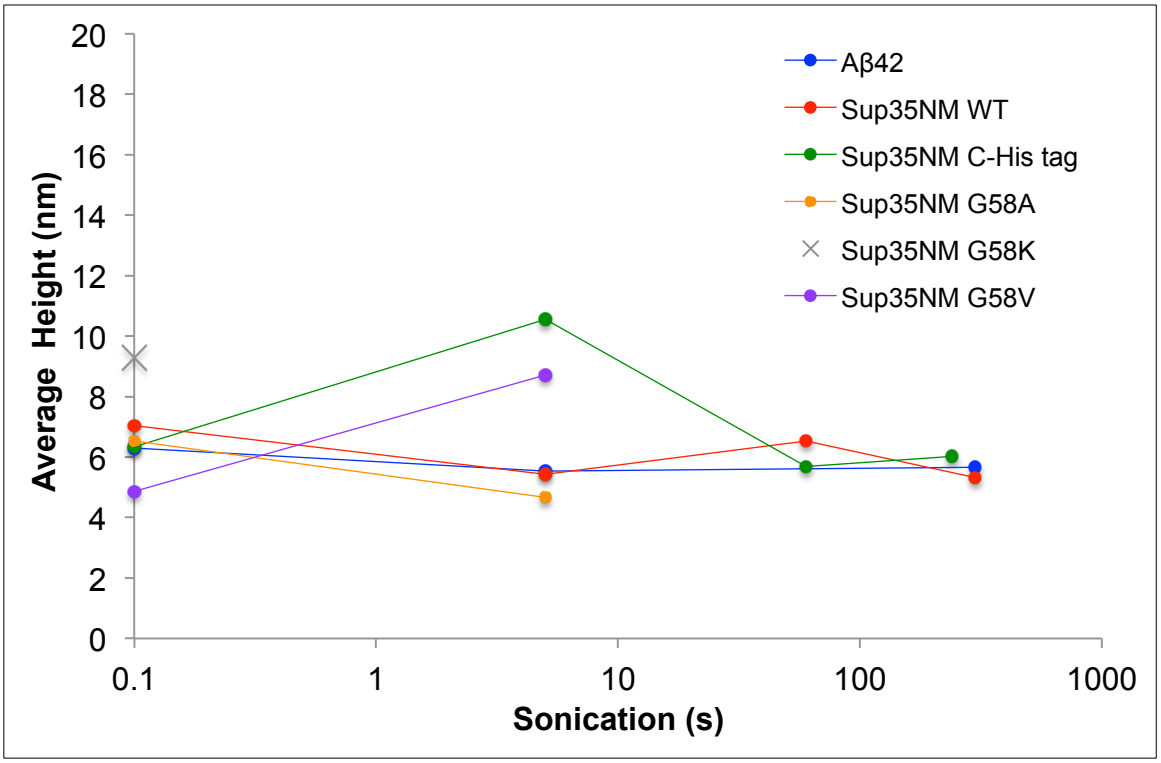

Summary of all the average particle heights (nm) collected. Across all proteins and sonication time point's average heights are maintained within the narrow range of 4.7 and 10.5 nm. Sonication time shown on a logarithmic scale.